B.Comp. Dissertation

Data-driven and Physics-inspired Machine Learning: Benchmarking Quantum-inspired Quadratic Unconstrained Binary Optimisation Solvers

By

Guo Yulong

Department of Computer Science

School of Computing

National University of Singapore

2023/2024

B.Comp. Dissertation

Data-driven and Physics-inspired Machine Learning: Benchmarking Quantum-inspired Quadratic Unconstrained Binary Optimisation Solvers

By

Guo Yulong

Department of Computer Science

School of Computing

National University of Singapore

2023/2024

Project No: H0811550
Advisor: Assoc Prof Stéphane Bressan

Deliverables:
Report: 1 Volume

Abstract

The quadratic unconstrained binary optimisation (QUBO) problem is a fundamental problem in combinatorial optimisation and offers a versatile framework that encapsulates various scientific and industrial optimisation challenges. However, the QUBO problem is NP-hard and is traditionally extremely difficult to solve efficiently due to its exponentially increasing search space. Our work aims to measure the performance of different quantum-inspired QUBO solvers that utilise quantum effects to search for optimal solutions. We benchmarked the D-Wave Quantum Annealer, Neural Network Quantum States (NNQS), and Quantum Approximate Optimization Algorithm (QAOA) solvers with classical commercial QUBO solvers. We used a dataset with various combinatorial problems—not-all-equal 3-satisfiability, max-cut, and the Sherrington-Kirkpatrick model, and the solvers were evaluated based on average normalised energy and success probability. Our results show that the D-wave and NNQS solvers outperform the QAOA solver but cannot match the performance of commercial QUBO solvers. However, when we match the solver runtimes, the D-wave solver showed promising performance for specific problem sizes. We also investigate the performance of the NNQS solver with different architectures and training algorithms. Our results show that the NNQS solver with a Restricted Boltzmann Machine and a continuous training algorithm performed best across all datasets.

Subject Descriptors:

10002950.10003714.10003716.10011136 Discrete optimization
10010405.10010432.10010441 Applied computing Physics
10010147.10010257.10010293.10010294 Neural networks

Keywords:

Quadratic unconstrained binary optimisation, Ising model, Quantum annealing, Neural network quantum states, Quantum Approximate Optimization Algorithm

Implementation Software and Hardware:

Tesla A100, Python, Tensorflow, Dimod, Qiskit

Acknowledgement

I would like to thank my friends and family for their constant support throughout the project. I would also like to thank my project advisor, Associate Professor Stéphane Bressan, research fellow Lu Jianlong, and past and present research group members for their invaluable guidance and support.

List of Figures

List of Tables

Table of Contents

Chapter 1

Introduction

1.1 Motivation

Quadratic unconstrained binary optimisation (QUBO) is a versatile combinatorial optimisation that can represent various combinatorial optimisation challenges and has vast applications in both operational research and industry (Kochenberger et al., 2014). Most problems that involve choosing a set of binary decisions to optimise an objective function can be expressed as a QUBO problem. Examples include max-cut problems, satisfiability problems, or even problems with more complex constraints, such as the travelling salesman problem (Lucas, 2014). However, QUBO problems are also NP-hard and are extremely hard to solve efficiently as the search space grows exponentially with the number of binary variables (Kochenberger et al., 2014). Traditionally, QUBO-solving methods were specialised for a specific problem domain to leverage the problem domain's unique characteristics, limiting the versatility and portability of these QUBO solvers (Glover, Kochenberger, Hennig, & Du, 2022).

The QUBO problem shares similarities with the Ising model in Physics, where instead of the binary variables in QUBO, we use spin variables, which are either -1 or $+1$. The two models are equivalent up to a change in variable domain, and the correspondence between the QUBO problem and the Ising model has opened the doors to solving QUBO problems with quantum-inspired methods (Glover et al., 2022). The equivalence enhances the problem domains that could be modelled as QUBO problems and also allows for QUBO problems to be solved by more general quantum-inspired solving methods (Glover et al., 2022).

With a broad range of classical and quantum-inspired methods available to tackle QUBO problems, it is imperative to consolidate and benchmark existing QUBO solvers to measure their performance when solving different kinds of QUBO problems across various types and sizes of QUBO problems.

1.2 Objectives

In the first section of the report, we aim to measure the performance of 3 quantum-inspired QUBO solvers:

1. Quantum Annealing
2. Neural Network Quantum States
3. Quantum Approximate Optimization Algorithm

We will also use classical solvers as a baseline for comparison with the quantum-inspired solvers. We will explore two classical solvers:

4. Fixstars Amplify QUBO Solver
5. GUROBI Optimizer

A range of problem types and sizes will be used as detailed in chapter 4. For each solver, we will calculate the success rate (probability of returning the best solution) and normalised energy (relative solution performance) across QUBO problems of different types and sizes. More details of the solvers and performance metrics are available in chapter 3 and chapter 4. The results are detailed in chapter 5.

In the second section of the report, we will explore how the parameters used for Neural Network Quantum States can affect their performance. We systematically compare two neural network architectures and three different training schedules highlighted in chapter 6. The results are detailed in chapter 6.

The results of the study will allow for a better understanding of the current landscape of quantum-inspired QUBO solvers and how they compare to state-of-the-art classical commercial solvers. We will also compare the performance of different architectures and training schedules for Neural Network Quantum States.

Chapter 2

Background and Preliminaries

2.1 Quadratic unconstrained binary optimisation

The quadratic unconstrained binary optimisation (QUBO) problem is defined as

$$\underset{x \in \{0,1\}^n}{\arg\min}\, x^\intercal Q x \tag{2.1}$$

where $Q \in \boldsymbol{M}_{n\times n}(\mathbb{R})$ is an upper triangular square matrix with real coefficients and x is a binary input vector (Kochenberger et al., 2014). The matrix Q characterises the QUBO problem, and $x^\intercal Qx$ is known as the objective function for the problem. Some characteristics of QUBO problems are summarised below:

- The possible input space grows exponentially with the size of the problem n, making the QUBO problem NP-hard and difficult to solve efficiently.
- In general, the solution of a QUBO problem does not need to be unique as multiple input x's can produce the same objective value.
- The density d of a QUBO problem is measured by the number of non-zero elements above the main diagonal of Q (quadratic terms). In general, a denser QUBO is more difficult to solve efficiently.

- We can also express a QUBO problem as a maximisation problem by finding $\arg\max_{x \in \{0,1\}^n} -x^\intercal Q x$.

Most problems that optimise an objective function concerning a set of binary decisions can be reformulated as a QUBO problem (Glover et al., 2022). Thus, the QUBO problem model has applications in a wide range of combinatorial optimisation problems such as Max-Cut (Kochenberger, Hao, Lu, Wang, & Glover, 2013), number partitioning (Alidaee, Glover, Kochenberger, & Rego, 2005), and machine scheduling problems (Alidaee, 2009). Once an optimisation problem is expressed in a QUBO format, we can utilise general QUBO-solving methods without specialising in a particular problem domain (Kochenberger et al., 2014). The following section will describe an example of a QUBO problem.

2.1.1 Example QUBO problem

Consider the objective function

$$f(x_1, x_2, x_3) = -8x_1 + 6x_2 + 3x_3 - 2x_1x_2 + 4x_2x_3 \tag{2.2}$$

where $x_1, x_2, x_3 \in \{0, 1\}$ and we want to minimise f over all possible (x_1, x_2, x_3). Since the variables are binary, $x_i^2 = x_i$ for all i, and we can redefine the objective function as:

$$f(x) = x^\intercal Q x, \text{ where } x = \begin{bmatrix} x_1 \\ x_2 \\ x_3 \end{bmatrix}, \; Q = \begin{bmatrix} -8 & -2 & 0 \\ 0 & 6 & 4 \\ 0 & 0 & 3 \end{bmatrix} \tag{2.3}$$

The coefficients for Q_{ii} are equal to the coefficient of x_i in the original objective function. The coefficients for Q_{ij} is the coefficient of x_ix_j for $i < j$ and 0 otherwise. This simple QUBO problem can be solved by enumerating all the possible inputs to obtain the optimal solution of $x_1 = 1, x_2 = 0, x_3 = 0$, and $f(1, 0, 0) = -8$.

We also show how a more complex combinatorial optimisation problem, the knapsack problem, can be converted to a QUBO problem in Appendix A. The knapsack problem has inequality constraints, which QUBO can also handle by introducing additional slack variables.

2.1.2 Practical applications

There are numerous practical scenarios where optimisation problems can be reformulated as QUBO problems.

- (Yarkoni et al., 2021) uses real-world data of the location of DB Schenker shipping hubs in Europe to solve the vehicle routing problem using a QUBO reformulation.
- (Lang, Zielinski, & Feld, 2022) uses a QUBO formulation to solve portfolio optimisation problems using data from stocks listed on the New York Stock Exchange.
- (Tavares, 2008) formulates an image binarisation method as a QUBO problem where the objective is to segment an image into its foreground and background, which has further possible medical applications to improve x-ray imaging.

These practical applications of the QUBO problem further motivate efficient methods for solving QUBO problems, some of which are detailed in chapter 3.

2.2 The Ising Model

The Ising model in Physics, proposed by Ernst Ising in 1925, can be thought of as a model of a magnet (Ising, 1925) and has been widely studied in Physics for its phase transition properties (Cipra, 1987). The Ising model serves as the bridge that allows for QUBO problems to be solved with quantum-based methods (Lucas, 2014). In the classical Ising model, a magnet consists of n molecules that are 'constrained to lie on the sites of a regular lattice' (Baxter, 2016). Each molecule i can be seen as a microscopic magnet that points along some axis and has a 'spin' (s_i) that is either $+1$ (parallel to the axis) or -1 (anti-parallel to the axis). With n particles, the system can have 2^n states, each corresponding to a configuration of the individual molecule spins.

2.2.1 Ising Hamiltonian

In quantum mechanics, the Hamiltonian of a system $\hat{H}$ is a linear operator that represents the total energy of a system and is a critical component that governs the evolution of the system (Griffiths & Schroeter, 2018). Section 2.3 discusses the Hamiltonian in greater detail. For this study, we can treat the Hamiltonian as a function of the quantum system that maps a quantum state to an energy level. A key property of the Hamiltonian matrix is that the possible energy levels of the system are precisely the eigenvalues of its Hamiltonian matrix, and the corresponding eigenvectors are the possible states mapped to a specific energy level (Zen et al., 2020).

In the Ising model with n particles, the Hamiltonian has two components — the external field term (characterised by $\mathbf{h} = (h_1, h_2, ..., h_n) \in \mathbb{R}^n$) and the interaction term between molecules (characterised by a strictly upper triangular matrix $\mathbf{J} \in \boldsymbol{M}_{n\times n}(\mathbb{R})$) (Lucas, 2014). We can express the Hamiltonian of an Ising model as a function of the n spins of the particles:

$$\hat{H}(s_1, s_2, ..., s_n) = -\sum_{1\leq i<j\leq N} J_{ij}s_is_j - \sum_{i=1}^{N} h_is_i \tag{2.4}$$

We can view $\mathbf{h}$ as the interaction of each particle with an external magnetic field and $\mathbf{J}$ as the coupling between pairs of spins. A positive J_{ij} term means that the energy is low when spins s_i and s_j are aligned, while a negative J_{ij} term means that the energy is low when the spins are anti-aligned. A large magnitude of h_i means the spin s_i tends to be either aligned or anti-aligned with an external magnetic field.

The Ising model was initially proposed to study phase transitions of the system at certain critical temperatures by solving for the system's ground state at different temperatures (Ising, 1925). To find the ground state—the state of spins that minimises the total system energy of the Ising model—we have to solve for $\arg\min \hat{H}(s_1, s_2, \ldots, s_n)$ for $s_1, s_2, \ldots, s_n \in \{0, 1\}$. This optimisation problem is equivalent to a corresponding QUBO problem up to a change in the variable domain (from spins to binary variables). The equivalence of the QUBO problem and the Ising model is one of the most significant properties of QUBO (Glover et al., 2022). The following subsections will explain converting a QUBO problem into an Ising model and vice versa.

2.2.2 Converting QUBO to Ising

Given a QUBO problem with QUBO matrix Q, we can use the conversion, $x_i = \frac{s_i+1}{2}, s_i \in \{-1, 1\}$ to change the spin variables into binary variables. The objective function $f(x)$ of the QUBO problem can be expressed as

$$
\begin{aligned}
f(x) &= f(x_1, ..., x_n) \\
&= \sum_{1 \le i < j \le n} Q_{ij}(x_i x_j) + \sum_{i=1}^{N} Q_{ii} x_i \\
&= \sum_{1 \le i < j \le n} \frac{1}{4} Q_{ij}(s_i + 1)(s_j + 1) + \sum_{i=1}^{N} \frac{1}{2} Q_{ii}(s_i + 1)
\end{aligned}
$$

If we group the constant terms into k and let $a_i = \sum_{1 \le j \le N, j \ne i} \frac{1}{4} Q_{\min(i,j)\max(i,j)} + \frac{1}{2} Q_{ii}$, we can express the objective function as:

$$
f(x) = \sum_{1 \le i < j \le n} \frac{1}{4} Q_{ij} s_i s_j + \sum_{i=1}^{N} a_i s_i + k
$$

Removing the constant k, which is irrelevant for optimisation, we can reformulate the QUBO problem as an Ising model with $h_i = -a_i$ and $J_{ij} = -\frac{1}{4} Q_{ij}$ for $i \ne j$. Finding the ground state for the Ising model is the same problem as finding $\arg\min_{x \in \{0,1\}^n} x^\intercal Q x$, and the solution to the ground state of the Ising model can be converted into a solution for QUBO problem using $x_i = \frac{s_i+1}{2}$. However, the optimal objective function value may differ due to the constant k.

2.2.3 Converting Ising to QUBO

Given the Hamiltonian of an Ising problem, we use the conversion $s_i = 2x_i - 1, x_i \in \{0, 1\}$ to change the spin variables into binary variables:

$$\begin{aligned}\hat{H}(s) &= - \sum_{1 \leq i < j \leq n} J_{ij} s_i s_j - \sum_{i=1}^{N} h_i s_i \\ &= - \sum_{1 \leq i < j \leq n} J_{ij} (2x_i - 1)(2x_j - 1) - \sum_{i=1}^{N} h_i (2x_i - 1) \\ &= - \sum_{1 \leq i < j \leq n} J_{ij} (4x_i x_j - 2x_i - 2x_j + 1) - \sum_{i=1}^{N} (2h_i x_i - h_i)\end{aligned}$$

If we group the constant terms into k and let $a_i = 2h_i + \sum_{1 \leq j \leq N, j \neq i} 2J_{\min(i,j)\max(i,j)}$, we can express the Hamiltonian as:

$$\hat{H}(s) = - \sum_{1 \leq i < j \leq n} 4J_{ij} x_i x_j - \sum_{i=0}^{N} a_i x_i + k$$

Removing the constant k, which is irrelevant for optimisation, we can reformulate the Ising model Hamiltonian as a QUBO matrix Q such that $Q_{ii} = -a_i$ and $Q_{ij} = -4J_{ij}$ for $i < j$. Finding $\arg\min_{x \in \{0,1\}^n} x^\intercal Q x$ is now the same problem as finding the ground state for the original Ising model, and the solution to the ground state of the Ising model can be mapped to a solution for QUBO problem using $s_i = 2x_i - 1$. However, the optimal objective function value may differ due to the constant k.

2.2.4 Solving for the ground state of the Ising model

In one and two-dimensional Ising models, each particle interacts with a small number of neighbours, and the ground state can be solved by calculating the partition function (Onsager, 1944) or by using the transfer matrix method (Kramers & Wannier, 1941). However, the Ising models of interest are of higher dimensions due to a large number of possible quadratic interactions, which render exact methods for finding their ground states computationally infeasible (Barahona, 1982). However, there are ways to approximate the ground state for higher dimensional Ising models which are explained in chapter 3.

2.3 Wave functions, Observables and Ansatzes

Quantum physics is built around wave functions and operators (Griffiths & Schroeter, 2018). Wave functions represent the state of the system and live in a infinite-dimensional Hilbert space, which is defined as the set of all square-integrable functions:

$$f(x) \text{ such that } \int_{-\infty}^{\infty} |f(x)|^2 \, dx < \infty$$

The properties of the Hilbert space allow the wave function, denoted as Ψ, to be normalised so that $\int_{-\infty}^{\infty} |\Psi|^2 \, dx = 1$. Under the statistical interpretation of quantum mechanics, $|\Psi(x)|^2$ would also represent the probability of a system being in state x once it is measured. The probabilistic nature of the wave function also implies that a wave function consists of a superposition of states. For this project, we will adopt the statistical interpretation and view the wave function as a probability distribution over all possible state configurations.

Quantum operators represent the observables—measurable system quantities such as position, momentum, or energy. Quantum operators are hermitian linear operators that act on a wave function to map states to observable values, which must be real. The operator's eigenvalues correspond to possible values of the represented quantity and are also real. When an operator acts on a wavefunction that exists as a superposition of multiple states, it returns an expected value of the observable instead, where $p(x) = |\Psi(x)|^2$. The Hamiltonian is the energy operator, and the eigenvalues of the Hamiltonian are all the possible energies a system could have. We will only be concerned with the Hamiltonian operator in this study.

For an Ising model, the wavefunction encodes the probabilities of each spin configuration, and the Hamiltonian maps a wavefunction to an energy expectation value, which is the expected energy.

An Ansatz is an educated guess for the solution to a problem, which often reduces the complexity or size of the problem (Blekos et al., 2024). When solving for the ground state of a wave function with variational methods, an Ansatz represents a subspace of the infinite-dimensional Hilbert space in which the wave function lives. It is important to ensure that the wave function is general enough to closely approximate the space of all solutions yet is specific enough to be optimised efficiently.

2.4 Sampling methods

Gibbs and Metropolis-Hasting sampling are Markov Chain Monte Carlo (MCMC) sampling methods used to sample from a probability distribution when direct sampling is infeasible. MCMC sampling methods are often used when training Neural Network Quantum States (NNQS) since we need the energy expectation value, but there are exponentially many states to average over. However, if we can sample from the probability distribution that the NNQS encodes, then we can obtain an unbiased estimate of the energy expectation value. We will first introduce Metropolis-Hasting sampling and then Gibbs sampling as a special case of Metropolis-Hasting sampling. We denote the complex probability distribution that we want to sample from as $\mathbb{P}(x)$.

Metropolis-Hasting sampling

Metropolis-Hasting sampling (Hastings, 1970) is often used when the underlying architecture of the NNQS is a Multilayer Perceptron (MLP) and proceeds as follows:

1. Initialise the MLP inputs with a random sample x.
2. Draw a new candidate sample x^* from the set of configurations with one flipped spin with a proposal distribution $q(x^*|x)$.
3. Accept the new candidate by replacing $x \leftarrow x^*$ with probability $\alpha = \min\left(1, \frac{\mathbb{P}(x^*)}{\mathbb{P}(x)}\frac{q(x|x^*)}{q(x^*|x)}\right)$.
4. Repeat steps 2 and 3 for a certain number of iterations.

For the NNQS, we usually use a uniform distribution for q, which leads to $\alpha = \min\left(1, \frac{\mathbb{P}(x^*)}{\mathbb{P}(x)}\right)$. When the proposal distributions are symmetric, the sampling method is also known as Metropolis sampling.

Gibbs sampling

Gibbs sampling (Geman & Geman, 1984) is used when the conditional distribution is easy to sample, which is the case when the underlying architecture for the NNQS is a Restricted Boltzmann Machine (RBM). Gibbs sampling proceeds as follows:

1. Initialise the visible layer of the RBM with a random sample $\mathbf{s}$.
2. Update the hidden layer by sampling from their respective conditional probability distribution given the current visible layer configuration with $\mathbb{P}(h_i = 1|\mathbf{s}) = \sigma(b_i + \sum_j W_{ji} s_j)$ where σ is the sigmoid function.
3. Update the visible layer by sampling from their respective conditional probability distribution given the current hidden layer configuration with $\mathbb{P}(s_i = 1|\mathbf{h}) = \sigma(a_i + \sum_j W_{ij} h_j)$ where σ is the sigmoid function.
4. Repeat steps 2 and 3 for a certain number of iterations.

The key benefit of Gibbs sampling on an RBM is that the visible units are conditionally independent given the hidden layer, and the hidden units are similarly conditionally independent given the visible layer. Thus, Gibbs sampling can be easily parallelised and accelerated using general purpose graphics processing units (GPUs).

Chapter 3

Methods for solving QUBO problems

This chapter reviews the different approaches used to solve QUBO problems. They can be broadly categorised as Classical, Quantum Annealing, Neural Network Quantum States, and Hybrid Quantum-Classical Algorithms.

3.1 Classical

Classical approaches search for solutions to QUBO problems without exploiting quantum properties. A typical classical approach is by exact diagonalisation of the corresponding Ising Hamiltonian (Zen, 2021). Exact diagonalisation solves for all the eigenvalues and eigenvectors and is also known as eigendecomposition, which is always possible for quantum Hamiltonians as they are represented by Hermitian matrices (Horn & Johnson, 1990). However, the runtime of exact diagonalisation scales exponentially with input problem size and becomes computationally infeasible once the matrix grows large (Zen, 2021). Since we are only interested in finding the smallest eigenvalue and the corresponding eigenvector, we can use iterative methods such as the Lanczos algorithm or the implicitly restarted Arnoldi method to find the smallest eigenvalue (Lanczos, 1950Lehoucq, Sorensen, & Yang, 1998). However, such methods also often run into stability issues. There are also branch and bound methods for solving QUBO problems, which aim to break down the QUBO into subproblems and build lower and upper bounds for the objective values (Otaki, Okada, & Yoshida, 2023). However, such methods are often built for specific classes of problems and may not apply to a general QUBO problem.

Due to the exponentially increasing search space, some classical methods aim to find approximate solutions to QUBO problems instead. One class of such methods relies on "heuristics" to search for optimal solutions (Dunning, Gupta, & Silberholz, 2018). Dunning et al.(2018) systematically reviewed and evaluated published heuristics for QUBO problems. However, heuristics often only work well for some QUBO problems and do not generalise well.

Another classical approximate method for solving QUBO problems is simulated annealing (SA). Simulated annealing (Kirkpatrick, Gelatt, & Vecchi, 1983) is a probabilistic method that starts with an initial trial state and a temperature T, which decreases slowly during the search. In each iteration, the algorithm samples neighbouring states of the current state and accepts the new sample based on the difference in energy, ΔE, between the current state and the new state. If $\Delta E < 0$, then the new sample is always accepted, and if $\Delta E \geq 0$, the new sample is accepted with a probability $\propto e^{-\frac{\Delta E}{T}}$. The algorithm to sample new states is adapted from the Metropolis-Hastings sampling method (Hastings, 1970), and the chance to explore poorer solutions allows the algorithm to escape local minima.

There are various classical approaches to solving QUBO problems, as they have been studied extensively. For a detailed survey of classical methods for solving QUBO problems, refer to (Punnen, 2022).

3.2 Quantum Annealing

Quantum annealing, introduced by Kadowaki and Nishimori (1998), finds the ground state configuration of Ising models. For a QUBO problem, we convert it to the equivalent Ising model and then use the *adiabatic theorem* to find its ground state configuration. The *adiabatic theorem* states that "a quantum system in its ground state will remain in the ground state, provided that the Hamiltonian governing the dynamics changes sufficiently slowly" (Yarkoni, Raponi, Back, & Schmitt, 2022Born & Fock, 1928). Suppose we can manipulate the final Hamiltonian of a quantum system to one that describes the Ising model of interest. In that case, we can find the ground state of the Ising model simply by measuring the final configuration of the quantum system.

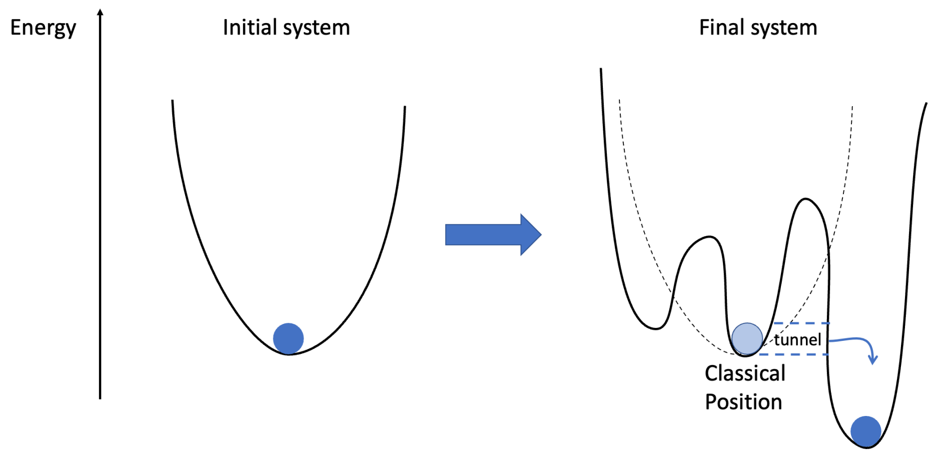

Figure 3.1: Energy landscape before (left) and after (right) quantum annealing

Quantum annealers first prepare a system in the ground state with a simple initial Hamiltonian H_0 (called the mixer or tunnelling Hamiltonian), with a simple energy landscape on the left of Figure 3.1. Then, the system Hamiltonian is slowly changed to a more complex form H_c (Lucas, 2014), with a complex energy landscape on the right of Figure 3.1. The Hamiltonian at any point $H(s)$ can be written as

$$H(s) = A(s)H_0 + B(s)H_c \tag{3.1}$$

where $s \in [0, 1]$ is the normalised anneal fraction and $A(s)$ and $B(s)$ are decreasing and increasing functions. At the start of the annealing, we should have $A(s) >> B(s)$, and at the end of the annealing, we should have $B(s) >> A(s)$. If the transition time is sufficiently large, the adiabatic theorem ensures that the system will remain in the ground state, which can then be measured to yield the desired ground state configuration of H_c (Yarkoni et al., 2022).

As H_0 usually consists of a transverse magnetic field and does not commute with the target Hamiltonian H_c, it allows for quantum tunnelling effects through energy barriers between classical states (Kadowaki & Nishimori, 1998). Quantum effects allow the wave function to remain at the ground state even when classical search methods may end up stuck in a local minimum. However, the adiabatic theorem requires an arbitrarily long anneal time to guarantee that the system remains in the ground state, which is not feasible for practical purposes. Current implementations of quantum annealing instead rely on a finite time approximation with repeated sampling to increase the success rate (Farhi et al., 2001).

Quantum annealing has been extensively studied and applied to solve many problems, such as scheduling problems (Rieffel et al., 2014), portfolio optimisation (Rosenberg et al., 2016), and quantum simulations (Harris et al., 2018). Even though there are significant roadblocks in scaling the currently limited hardware capabilities (Yarkoni et al., 2022), with debate on whether quantum annealing will eventually run faster than classical search methods (Lucas, 2014), there is hope that these challenges can be tackled soon with the rapid progress made in quantum computing technology. D-wave is the current leading commercial provider of quantum annealing hardware (D-Wave Systems, 2024b).

3.3 Neural-Network Quantum States

Carleo and Troyer (Carleo & Troyer, 2017) introduced a neural-network-based method for modelling the wave function of a target quantum system known as *neural-network quantum states* (NNQS). The authors used the approach to find the ground state and time evolution of the Ising and Heisenberg models in Physics. The NNQS is used as an Ansatz to approximate the wave function, which can be viewed as a probability distribution of a system (Zen, 2021). The more general method of using an Ansatz as a trial wave function and minimising its energy through Monte Carlo sampling is also known as variational Monte Carlo.

The theoretical foundations for NNQS to approximate wave functions of quantum systems rely on the Kolmogorov–Arnold representation theorem (Kolmogorov, 1957), which implies that neural networks can represent all multivariate, smooth functions. Since the wave function generally satisfies these requirements, we can expect that a neural network can reasonably approximate the wave function of a quantum system (Carleo & Troyer, 2017).

The original NNQS architecture utilised a Restricted Boltzmann Machine (RBM) as its neural network (Carleo & Troyer, 2017). The RBM, shown in Figure 3.3, is an energy-based generative model that has three components: a visible layer $\boldsymbol{s}$ with n nodes, a hidden layer $\boldsymbol{h}$ with m nodes, and a weight matrix $\mathbf{W}$. The number of hidden nodes is generally a multiple of the number of visible nodes, and the ratio $\alpha = \frac{m}{n}$ is a hyperparameter of the model. Each visible node s_i is connected to every hidden node h_j with a certain weight W_{ij}, but there are no connections within the visible or hidden layer. In other words, the visible and hidden nodes of the RBM form a bipartite graph.

When approximating the wave function of an Ising model, each visible node s_i represents the spin of a particle in the Ising model and can only take on the values of 1 and -1 (Carleo & Troyer, 2017). The representation of the wave function by the RBM can

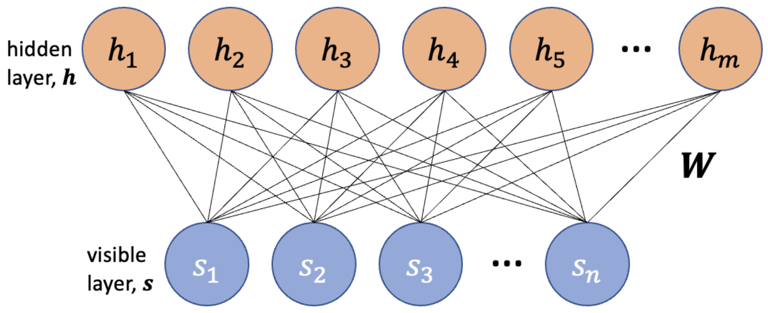

Figure 3.2: Structure of Restricted Boltzmann Machine

be expressed as:

$$\hat{\Psi}(\boldsymbol{s}; \boldsymbol{\theta}_{rbm}) = \sum_{h} e^{\sum_i a_s s_i + \sum_j b_j h_j + \sum_{i,j} W_i s_i h_j} \tag{3.2}$$

where $\boldsymbol{\theta}_{rbm} = \{\boldsymbol{a}, \boldsymbol{b}, \boldsymbol{W}\}$ are the biases and weights of the RBM (Carleo & Troyer, 2017). The network weights $\mathbf{W}$ are usually updated by performing Gibbs sampling, calculating the average energy of sampled configurations, and using gradient-based optimisers or the stochastic reconfiguration method to derive weight updates (Zen, 2021).

Other neural network architectures, such as the Multilayer Perceptron (MLP), can also be used for NNQS. An MLP model is a feedforward artificial neural network that consists of an input layer $\boldsymbol{x}$, one or more hidden layers, and an output layer. Each layer is fully connected to the next layer with certain weights, and each node has a non-linear activation function σ such as the sigmoid or ReLU function.

When approximating the wave function of an Ising model, each input node x_i represents the spin of a particle in the Ising model, and the output nodes represent the value of the wave function. If we assume the wave function to be real and positive, then only one output node is needed to represent the real part of the wave function (Carleo & Troyer, 2017). With a complex wave function, we could use two output nodes that represent the real and imaginary components of the wave function. With one hidden layer, the MLP representation of the wave function can be expressed as:

$$\hat{\Psi}(\boldsymbol{x}; \boldsymbol{\theta}_{mlp}) = \sigma_{out}\left(\boldsymbol{W}_{out}\, \sigma_{hidden}\left(\boldsymbol{W}_{hidden}\boldsymbol{x} + \boldsymbol{b}_{input}\right) + \boldsymbol{b}_{hidden}\right) \tag{3.3}$$

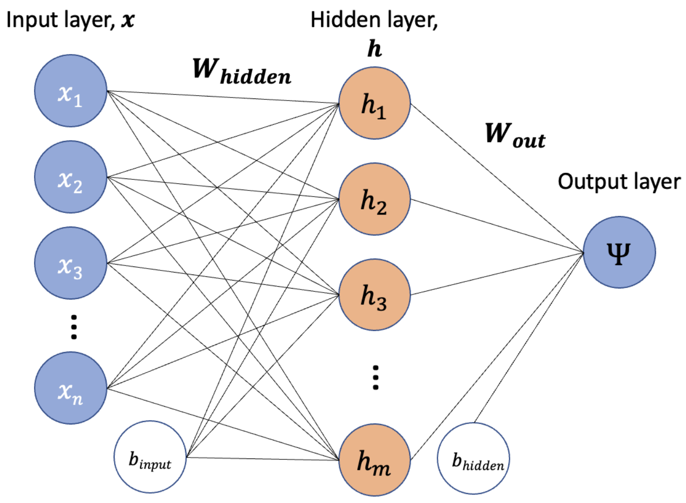

Figure 3.3: Structure of Multilayer Perceptron with one hidden layer and one real-valued output node

where $\boldsymbol{\theta}_{mlp} = \{\boldsymbol{W}_{hidden}, \boldsymbol{b}_{input}, \boldsymbol{W}_{out}, \boldsymbol{b}_{hidden}\}$ are the weights and bias of the MLP and $\sigma_{out}, \sigma_{hidden}$ are the non-linear activation functions of the nodes (Carleo & Troyer, 2017). The MLP is trained similarly to the RBM, except that a more general sampling method, the Metropolis-Hasting algorithm, is used (Zen, 2021).

3.4 Hybrid quantum-classical

Hybrid quantum-classical methods are designed to use current limited quantum computing resources by integrating them with classical optimisers to solve QUBO problems (Zhou, Wang, Choi, Pichler, & Lukin, 2020). One such algorithm is the Quantum Approximate Optimization Algorithm (QAOA) (Farhi, Goldstone, & Gutmann, 2014). Like NNQS, QAOA aims to find an approximation of the ground state of an input Hamiltonian using an Ansatz. The Ansatz used is a gate-based quantum circuit with $2p$ variational parameters $\gamma_1, \beta_1, \ldots, \gamma_p, \beta_p$ optimised with a classical optimiser (Willsch, Willsch, Jin, De Raedt, & Michielsen, 2020). For a problem size n. the algorithm first prepares a quantum state $|+\rangle^{\otimes n}$ in uniform superposition by applying the Hadamard gate to n qubits. The trial wave function is then constructed with:

$$\hat{\Psi}(\boldsymbol{\gamma}, \boldsymbol{\beta}) = U_B(\beta_p)U_C(\gamma_p)...U_B(\beta_1)U_C(\gamma_1)|+\rangle^{\otimes n} \tag{3.4}$$

$$U_C(\gamma) = e^{-i\gamma H_c} \tag{3.5}$$

$$U_B(\beta) = e^{-i\beta H_0} \tag{3.6}$$

Using the time-independent Schrödinger equation, we can see that U_c and U_B are operators that evolve the state with the Hamiltonian H_c (problem Hamiltonian) and H_0 (an easy-to-implement, mixing Hamiltonian) for time intervals $\boldsymbol{\gamma}$ and $\boldsymbol{\beta}$. At the same time, the parameter p determines the number of time evolutions of the final state (Willsch et al., 2020).

Each operation in the mixing Hamiltonian is implemented with a single rotation gate R_X while the two-qubit operations in the problem Hamiltonian are implemented with a 2-qubit R_{ZZ} gate (Blekos et al., 2024). A circuit diagram of the QAOA circuit is shown in Figure 4.3 with the Hadamard gates on the left, repeated blocks of U_c and U_B operators and a measurement of the final qubit states. The state is then measured repeatedly to obtain samples of the qubit configurations, the energies of the samples are calculated, and $\boldsymbol{\gamma}$ and $\boldsymbol{\beta}$ are optimised to minimise the average energy of the samples. The final solution can be determined by repeatedly sampling from the trial wave function with the optimised parameters.

QAOA can be regarded as a discretised version of Quantum Annealing (Blekos et al., 2024). In the noisy intermediate-scale quantum (NISQ) era, quantum computers are not yet stable enough to reliably run deep and complex quantum circuits (Blekos et al., 2024). Hybrid methods could serve as the intermediate solution for optimisation problems on quantum computers. In contrast to quantum annealing, which can only be run on specialised quantum annealing devices, QAOA can be implemented on a general gate-based quantum computer (Kurowski et al., 2023).

Chapter 4

Methodology

This chapter explains the methodology employed in our study, which includes the solvers, datasets, and evaluation metrics.

4.1 Solvers

We will employ five QUBO solvers for the study:

1. D-Wave Quantum Annealing
2. Neural Network Quantum States (NNQS)
3. Quantum Approximate Optimization Algorithm (QAOA)
4. GUROBI Optimizer
5. Fixstars Amplify QUBO Solver

The following sections will provide more information on the solvers.

4.1.1 D-Wave Quantum Annealing

We will use quantum annealers from D-Wave Systems, which produce the most popular commercially available quantum annealing hardware. The annealers are accessed with D-

Wave's Solver API and use radio frequency superconducting quantum–interference device (rf-SQUID) qubits to represent spin variables during the annealing process (Yarkoni et al., 2022). External magnetic fields represent the linear interactions (h terms), while couplers help entangle pairs of qubits to represent the interaction between qubits (J terms). The qubits are arranged in the Pegasus graph topology shown in Figure 4.1 that allows up to 15 couplers per qubit (Yarkoni et al., 2022).

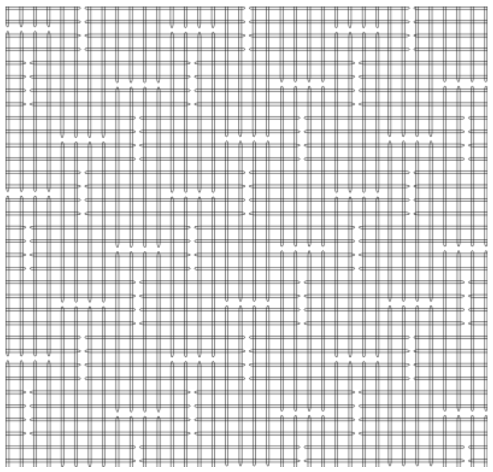

Figure 4.1: A view of the D-Wave pegasus topology. Each line represents a qubit, and intersections represent available couplers. Each qubit can only be coupled to at most 15 other qubits. (McGeoch & Farré, 2021)

The experiments will be conducted with the D-Wave Advantage 4.1 QPU, which has up to 5640 qubits and 40484 couplers (McGeoch & Farré, 2021). Given a target QUBO problem to solve, the process for using a D-Wave annealer is as follows:

1. **Problem Definition** QUBO problem is first converted to its corresponding Ising model.

2. **Minor Embedding** As the D-Wave quantum processing unit shown in Figure 4.1 is not fully connected, a single spin variable may need to be represented by multiple qubits called a *chain*, which are forced to return the same value with large interaction terms (D-Wave Systems, 2024b). The EmbeddingComposite class in the D-Wave

library performs the embedding.

3. **Programming** The parameters of the annealing process are set, which consists of the linear term for each qubit (with an external magnetic field acting on each qubit) and coupler strength (represents variable interaction between spins).

4. **Initialization** The QPU is initialised in the ground state of the initial Hamiltonian, which is usually a superposition of all possible states.

5. **Annealing** The system evolves with a time-varying Hamiltonian:
$$H(s) = -\frac{A(s)}{2}\left(\sum_i \hat{\sigma}_x^{(i)}\right) + \frac{B(s)}{2}\left(\sum_i h_i \hat{\sigma}_z^{(i)} + \sum_{i>j} J_{i,j}\hat{\sigma}_z^{(i)}\hat{\sigma}_z^{j)}\right) \tag{4.1}$$
where s is the normalised anneal fraction and $A(s), B(s)$ are annealing functions shown in Figure 4.2. We will use the default annealing time of $20\mu s$.

6. **Readout of solution** The spin values of the qubits are measured and stored as a possible solution.

7. **Resample** As finite-time quantum annealing does not guarantee optimality, we repeat the annealing and sampling process for 1000 iterations and use the sample with the lowest energy as the candidate solution.

4.1.2 Neural-Network Quantum States

We will adopt the Python library MAPALUS for implementing Neural-Network Quantum States (Zen, 2021). MAPALUS uses the Tensorflow library and enables parallel execution on general-purpose graphics processing units for quicker sampling. We will use the Restricted Boltzmann Machine with $5n$ hidden nodes and the sigmoid activation function as the underlying architecture for the NNQS.

To solve a QUBO problem, the NNQS simulates the D-Wave quantum annealing process on a classical computer with a time-dependent Hamiltonian that follows Equation 3.1.

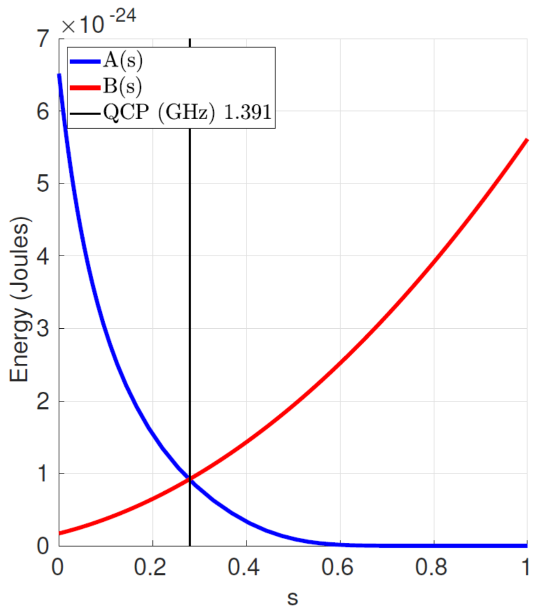

Figure 4.2: Annealing functions $A(s)$ and $B(s)$ as a function of the normalised anneal fraction s. $A(s) >> B(s)$ when $s = 0$ and $B(s) >> A(s)$ when $s = 1$. (McGeoch & Farré, 2021)

Since the equations for $A(s)$ and $B(s)$ are unavailable, we employ a curve-fitting process to obtain analytical functions from the discrete points provided by D-Wave. The annealing functions used are:

$$A(s) = 1.11e^{-7.06s} + -0.00569 \tag{4.2}$$

$$B(s) = 0.680s^2 + 0.288s + 0.0305 \tag{4.3}$$

The curve fitting process is detailed in Appendix B. The NNQS will be trained with a progressive training schedule that mimics the quantum annealing process and follows Algorithm 1. $\hat{H}_c$ is the problem Hamiltonian and $\hat{H}_0$ is a Hamiltonian with linear biases as 1 and no quadratic terms. The normalised anneal fraction s is increased in small steps while the NNQS is trained to convergence, which simulates the slow change in the system Hamiltonian during quantum annealing. Like quantum annealing, the NNQS remains in the ground state throughout the training as it is trained to convergence.

The training process of the NNQS involves updating the parameters, $\boldsymbol{\theta}$, with a Vari-

Algorithm 1 NNQS Progressive Training

```
Require: Problem Hamiltonian $\hat{H}_c$
Ensure: Trained NNQS
  Initialize NNQS with random weights;
  for $s \in [0.1, 1.0]$ step 0.1 do
      Set $H(s) \leftarrow A(s)\hat{H}_0 + B(s)\hat{H}_c$;
      Train NNQS on $H(s)$ until convergence or until epoch limit of 100 is reached;
```

ational Monte Carlo approach to minimise the energy expectation value. The training algorithm is described as follows:

1. Sample a set of 1000 configurations **s** from the probability distribution defined by the NNQS, $\mathbb{P}(s) = |\Psi(s; \theta)|^2$, with Gibbs sampling section 2.4.

2. Calculate an unbiased estimate of the energy expectation value with the average energy of the sampled configurations.

3. Compute the gradients of the energy expectation value with respect to the NNQS parameters using backpropagation.

4. Update the parameters with Root Mean Squared Propagation (RMSprop), a gradient-based optimiser, with a learning rate of 0.001 (Tieleman, 2012).

5. Repeat steps 1-4 for 1000 iterations or until convergence is reached.

The derivation of the gradients is detailed in the appendix of (Carleo & Troyer, 2017). The candidate solution will be the best among the 1000 configurations sampled from the final NNQS. All NNQS experiments were run on a 32 Core AMD 7543P Processor and an NVIDIA A100 40GB GPU with 500GB of RAM.

4.1.3 Quantum Approximate Optimization Algorithm

We will implement QAOA in Qiskit, an open-source software development kit for quantum computing, with $p = 1$ using a backend hosted on the IBM Quantum Platform (IBMQ) (Qiskit contributors, 2023). We will utilise the IBMQ simulator, `ibmq_qasm_simulator`, a general-purpose simulator for quantum circuits that can handle up to 32 qubits. Even though IBMQ allows for access to quantum computers, it is limited by long wait times (> 5 hours for each problem) and is infeasible for a benchmarking experiment. To measure the optimal performance of the QAOA algorithm, we will assume an ideal circuit without a quantum noise model. We will use the default mixing Hamiltonian of $\hat{H}_0 = \sum_i \hat{\sigma}_x^{(i)}$ and the Qiskit transpiler to optimise the decomposition of the operators into their individual parametrised quantum gates as shown in Figure 4.3 (IBM, 2024).

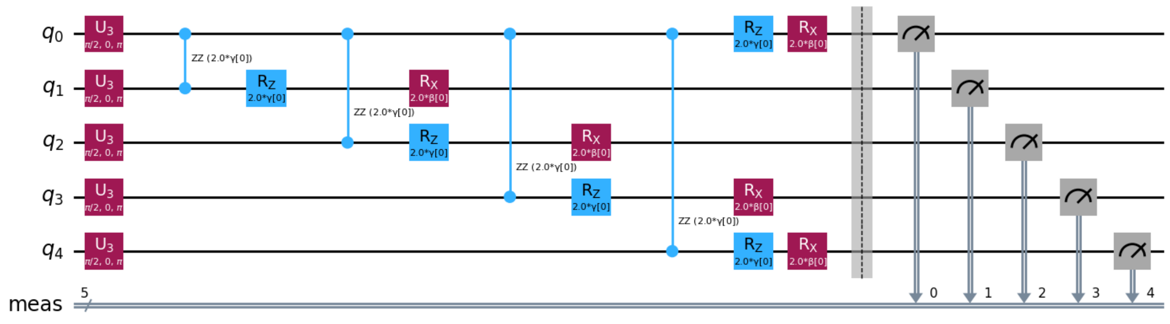

Figure 4.3: Circuit diagram of the QAOA circuit with $p = 1$ with $n = 5$. The Hadamard gates, problem Hamiltonian operator (R_z and R_{zz} gates), mixing Hamiltonian operator (R_x gates), and measurement gates are shown from left to right.

The parameters $(\boldsymbol{\gamma}, \boldsymbol{\beta})$ are updated to minimise the energy expectation value. The training algorithm is described as follows:

1. Initialise the circuit in the initial state $|+\rangle^{\otimes n}$ where each qubit is in a superposition state. Initialise γ and β with values sampled from a standard Gaussian normal distribution.

2. Construct the operators $U_C(\gamma), U_B(\beta)$ with γ, β, which consists of different quantum gates.

3. Repeatedly sample the final states of the qubits and calculate an unbiased estimate of the energy expectation value as the average energy of the sampled configurations.

4. Use a classical derivative-free optimiser Constrained Optimisation by Linear Approximation (COBYLA) to optimise the parameters γ, β to minimise the energy expectation value.

5. Repeat steps 2-4 for some iterations or until convergence is reached.

We will repeatedly sample the final optimised circuit 1000 times, and the candidate solution will be chosen as the best solution among the sampled configurations. The QAOA solver is accessed with the IBM Quantum Qiskit Runtime API and is run on the IBMQ cloud servers.

4.1.4 GUROBI Optimizer

The GUROBI optimiser is a state-of-the-art classical commercial solver (Gurobi Optimization, LLC, 2023). The GUROBI optimiser uses a branch and bound algorithm that first relaxes the integer constraint of the QUBO problem, then branches into subproblems based on variables that violate the constraints. As the GUROBI optimiser supports QUBO problems, we construct the QUBO matrix directly and run the optimiser locally for 10 minutes for each input problem. If the optimiser finishes before the cutoff, the candidate solution is guaranteed to be the optimal configuration. Otherwise, we would use the best solution within the cutoff time as the candidate solution. All experiments were run on a 32 Core AMD 7543P Processor using Gurobi Optimizer version 10.0.3.

4.1.5 Fixstars Amplify QUBO Solver

The Fixstars Amplify QUBO solver is a commercial simulated annealing-based QUBO solver that runs in parallel on GPUs on Fixstars' remote servers (Dunning et al., 2018). As the Fixstars solver supports QUBO problems, we submit the QUBO matrix using the Fixstars API and run the solver with the highest allowed time limit of 100 seconds for each input problem.

4.2 Benchmark datasets

We use three randomly generated problem sets to benchmark our QUBO solvers: not-all-equal 3-satisfiability (NAE3SAT), max-cut, and the Sherrington-Kirkpatrick (SK) model. These problems were chosen as they are commonly used in QUBO experiments to represent NP-hard problems and are relatively straightforward to encode into QUBO form. The NAE3SAT and max-cut problem sets are macro benchmarks (application-based) to represent practical combinatorial optimisation problems. In contrast, the SK model problem set is a microbenchmark designed as a difficult QUBO problem set. Each problem set comprises problems of 13 sizes, ranging from 10 to 300[1]. 20 different random problems are generated[2] for each problem size for a total of 260 problems per problem set. Each problem is first formulated in either the QUBO or Ising form, and the conversion between them follows subsection 2.2.2 and subsection 2.2.3.

Not-all-equal 3-satisfiability (NAE3SAT)

The NAE3SAT problem is a variant of the boolean satisfiability problem where each problem instance consists of n boolean variables $(x_1, x_2, ..., x_n)$ and m clauses that each combine three literals, which can be a variable or its negation. The objective is to find an

[1]$n \in [10, 15, 20, 25, 30, 35, 50, 75, 100, 150, 200, 250, 300]$

[2]random seed is chosen to be from $0 - 19$

assignment of boolean values such that the three values in each clause are not all the same, i.e., each clause has at least one true and one false value. We generate random NAE3SAT problems with $\rho = \frac{m}{n} = 2.1$, where NAE3SAT problems are known to transition from being satisfiable to unsatisfiable (Achlioptas, Chtcherba, Istrate, & Moore, 2001), using the random_nae3sat generator from the dimod Python library, which uniformly samples 3-variable clauses with replacement (D-Wave Systems, 2024d).

To convert a NAE3SAT problem into an Ising problem, we represent each boolean variable as a spin variable and turn each clause into a Hamiltonian term. For example, the clause $(x_1, x_2, \neg x_3)$, becomes the Hamiltonian term $H(s_1, s_2, s_3) = s_1 \cdot s_2 + s_2 \cdot (-s_3) + s_1 \cdot (-s_3)$ which has a value of 3 when $x_1 = x_2 = \neg x_3$ and -1 otherwise. The final Hamiltonian $\hat{H}_c$ is simply a sum of the individual Hamiltonian terms for each clause.

Max-cut

The max-cut problem aims to find a partition of the vertices of a graph $G = (V, E)$ into V_0, V_1 with $V = V_0 \cup V_1$ and $V_0 \cap V_1 = \emptyset$, to maximise the number of edges crossing V_0 and V_1. We will use the Erdos-Renyi model to generate random graphs with n vertices and a probability $p = 0.25$ for each edge to be in E.

To convert a max-cut problem into a QUBO problem, we represent the assignment of each vertex as a binary variable ($x_v = i$ if $x \in V_i$) and use the objective function $f(\mathbf{x}) = \sum_{e=(u,v)\in E} -x_u - x_v + 2x_u x_v$, where each term has a value of -1 when $x_u \neq x_v$ and 0 otherwise. When the cut value is maximised, $f(\mathbf{x})$ is minimised.

Sherrington-Kirkpatrick (SK) model

The Sherrington Kirkpatrick (SK) model is an Ising problem with a random Hamiltonian of the form $\hat{H}_c = \frac{1}{\sqrt{n}} \sum_{1\leq i<j\leq n} J_{ij} s_i s_j$ where $J_{ij} \sim \mathcal{N}(0, 1)$ are independent standard Gaussian variables. The energy landscape of the SK model is complex as it has expo-

nentially many local minima with a unique global minimum separated by high energy barriers (D. J. Thouless & Palmer, 1977). This many-valley structure implies that finding the exact solution of the model is challenging. We generate random Gaussian variables with a random normal generator from the NumPy Python library.

4.3 Performance evaluation

We use two metrics to evaluate the performance of the solvers, which are calculated separately for each problem type and size:

1. The success probability, which is the probability of finding a solution with the lowest energy among all solutions found by the 5 solvers. Since we are generating 20 problems of each type and size, the success probability for each solver is:

$$\bar{p} = \frac{\text{number of lowest energy solutions found}}{20} \tag{4.4}$$

2. The average normalized energy, used in (Willsch et al., 2020), which is:

$$\bar{r}_{solver} = \frac{1}{20}\sum_{i=1}^{20} \frac{E^i_{max} - E^i_{solver}}{E^i_{max} - E^i_{min}} \tag{4.5}$$

   where E^i_{max} and E^i_{min} are the energies of the worst and best solutions found by all solvers for problem i, and E^i_{solver} is the energy that the solver found for problem i. Note that if a solver finds the best solution, it gets a normalised energy of 1; if it finds the worst solution, it gets a normalised energy of 0. All solvers get a normalised energy of 1 if all solutions have the same energy.

The average normalised energy measures the quality of the solutions produced by the solvers, while the success probability measures the solvers' ability to find the best solution.

Chapter 5

Benchmarking QUBO solvers

This chapter first introduces related benchmarking work for QUBO problems and solvers. Then, we present the results of our benchmarking experiment.

5.1 Related Benchmarking Work

One of the first benchmarking works for quantum annealing was conducted by Denchev et al. (2016), who measured the performance of D-Wave quantum annealing using a carefully crafted problem named weak-strong cluster networks, which has "tall and narrow energy barriers separating local minima". For such problems with $\sim 10^3$ variables, quantum annealing is expected to be $\sim 10^8$ times faster to return the optimal solution compared to simulated annealing running on a single processor core. Vert, Sirdey, and Louise (2021) used the maximum cardinality matching problem, a problem that is specially designed to be difficult for simulated annealing, and found that the D-Wave quantum annealer performs poorly compared to simulated annealing. Huang et al. (2023) conducted a recent benchmark study comparing the D-Wave quantum annealer, Fujitsu Digital Annealer and the GUROBI solver on the warehouse assignment problem. While the D-Wave annealer was the fastest solver, it yielded the worst solutions among all solvers tested.

For the QAOA solver, Willsch et al. (2020) evaluated the performance of QAOA on the IBMQ backend and the D-Wave solver using instances of MaxCut and 2-satisfiability problems with up to 18 variables. The performance of the QAOA algorithm is inconsistent and underperforms quantum annealing in their problem set. Zhou et al. (2020) compared simulated quantum annealing with QAOA with large values of p and found that QAOA could find optimal solutions quicker than quantum annealing. However, the study only used small problems with sizes of $10-18$ and the parameter optimisation time for QAOA was omitted. More recently, Pelofske, Bärtschi, and Eidenbenz (2023) also compared the performance of QAOA on the IBMQ backend and D-Wave quantum annealing on randomly generated Ising problems with cubic interaction terms and found that quantum annealing had superior performance over QAOA for all problem sizes. Lykov et al. (2023) compared the QAOA solver with the GUROBI solver for max-cut problems on 3-regular graphs. They suggested that the QAOA solver would need to use $p > 11$ to match the performance of classical solvers for large graphs, which is greatly beyond what current quantum hardware can achieve.

Gomes, McKiernan, Eastman, and Pande (2019) showed that the NNQS solving method with an RBM architecture produces high approximation ratio solutions for the max-cut problem with graph sizes of up to 256. Khandoker, Abedin, and Hibat-Allah (2023) uses recurrent neural networks as the NNQS architecture for the max-cut and travelling salesman problem and found that it outperforms simulated annealing. However, there has yet to be a direct study that compares quantum annealing, QAOA, and NNQS.

5.2 Results and Discussion

We present the performance metrics from the benchmarking experiment for each dataset, accompanied by error bars representing the unbiased standard error of the mean. Graphs with problem sizes on the x-axis are plotted with a log scale.

5.2.1 NAE3SAT

Performance by size for the NAE3SAT dataset is shown in Figure 5.1, and average performance is shown in Figure 5.2. The D-Wave and NNQS solvers could solve problems up to $n = 300$. However, multiple embedding requests were required for problems of size 300 for the D-Wave solver, which suggests that $n = 300$ might be near the D-Wave solver's size limit for the NAE3SAT problem. The QAOA solver is limited to problems of up to $n = 30$.

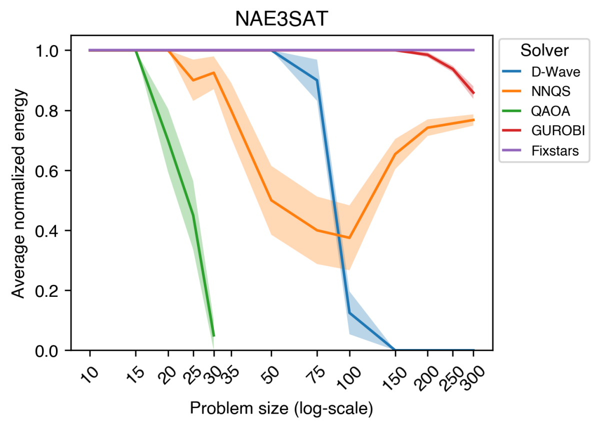

(a) Normalized energy

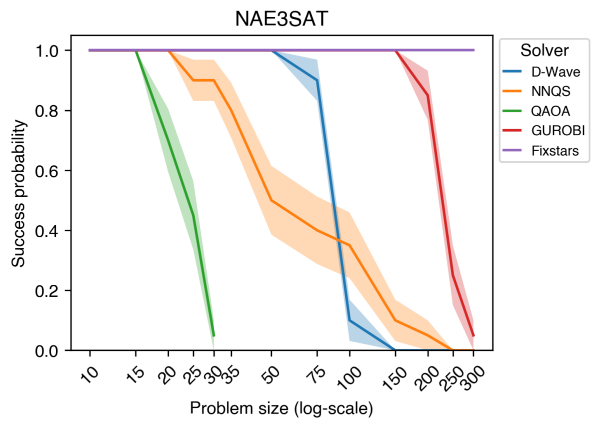

(b) Success probability

Figure 5.1: Performance of different solvers for NAE3SAT by problem size

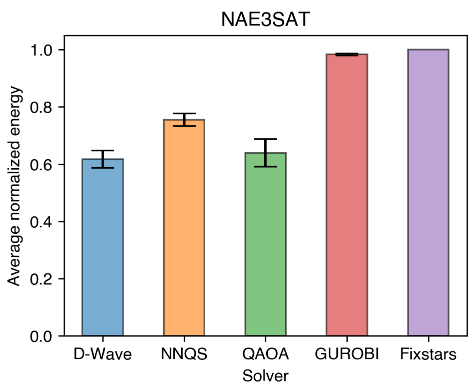

(a) Normalized energy

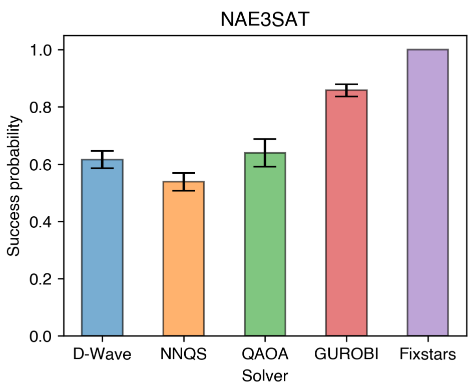

(b) Success probability

Figure 5.2: Average performance of different solvers for NAE3SAT

The D-Wave solver performs well up to $n = 50$ with a success probability of 1. For larger problem sizes, the performance of the D-Wave solver drops off sharply. The NNQS solver performs well up to $n = 20$, with the success probability and normalised energy gradually decreasing as the problem size increases until $n = 300$. The QAOA solver performs well up to $n = 15$, and performance decreases until $n = 30$. Among the classical solvers, the Fixstars solver performs better than the GUROBI solver at larger problem sizes (> 150). Both classical solvers outperform the quantum-inspired solvers.

Overall, the NNQS has the highest average normalised energy among the three quantum-inspired solvers but has the lowest success probability, which is likely due to it being able to solve problems of larger sizes that the D-Wave Annealer and QAOA solver cannot handle. The QAOA solver has the highest success probability but can only handle problems up to $n = 30$. Both classical solvers outperform the quantum-inspired solvers.

5.2.2 Max-cut

Performance by size for the max-cut dataset is shown in Figure 5.3, and average performance is shown in Figure 5.4. The D-Wave solver could only handle max-cut problems of sizes up to $n = 150$ due to the need for minor embedding onto the QPU's pegasus topology. The max-cut problem requires $\sim 0.25n$ edges per vertex, making the embedding challenging for large n. The NNQS solver could solve problems up to $n = 300$. The QAOA solver is limited to problems of up to $n = 30$.

The D-Wave solver performs well up to $n = 30$ with a success probability of 1, and performance drops off sharply for larger problems. The NNQS solver performs well until $n = 150$, although the success probability decreases for problem sizes over 50. The NNQS solver finds better solutions than the D-Wave solver but cannot find the best solution compared to the classical solvers. The QAOA solver performs well only for $n = 10$, with decreasing performance until $n = 30$. The Fixstars solver consistently performs better

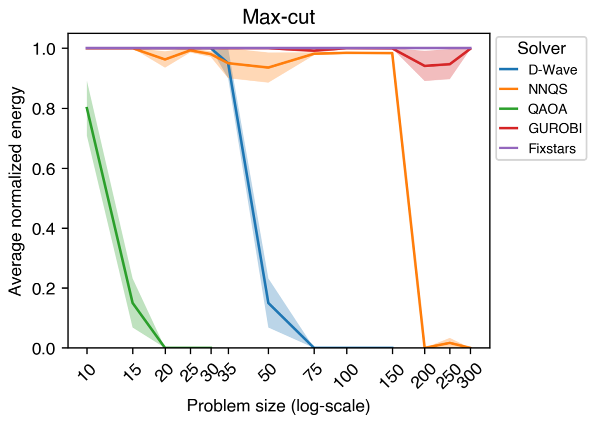

(a) Normalized energy

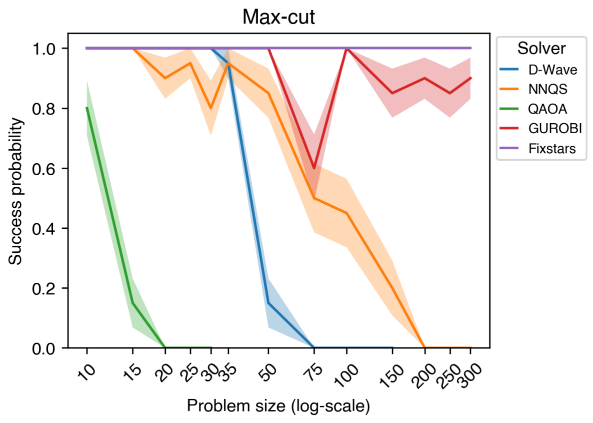

(b) Success probability

Figure 5.3: Performance of different solvers for max-cut by problem size

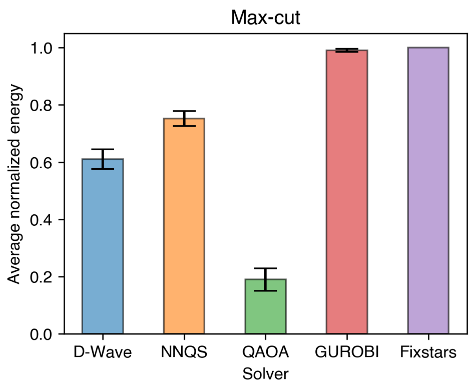

(a) Normalized energy

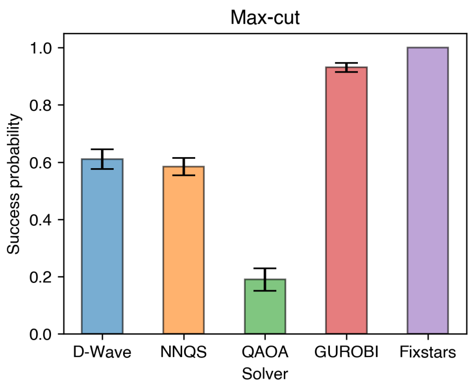

(b) Success probability

Figure 5.4: Average performance of different solvers for max-cut

than the GUROBI solver, while both classical solvers outperform the quantum-inspired solvers.

Overall, the NNQS has the highest average normalised energy among the three quantum-inspired solvers and has a slightly lower success probability than the D-Wave solver. The QAOA solver performs poorly in both metrics. Both classical solvers outperform the quantum-inspired solvers.

5.2.3 SK model

Performance by size for the SK model dataset is shown in Figure 5.5, and average performance is shown in Figure 5.6. The D-Wave solver could only solve problems up to $n = 150$ due to the need for minor embedding onto the pegasus topology. The SK model is fully connected, which makes embedding difficult for large n. The NNQS solver could solve problems up to $n = 300$. The QAOA solver is limited to problems of up to $n = 30$.

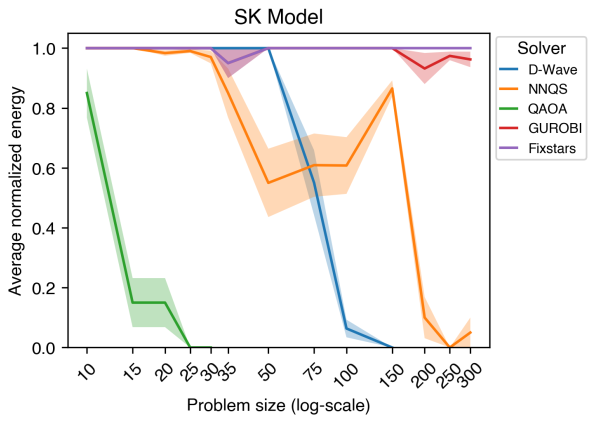

(a) Normalized energy

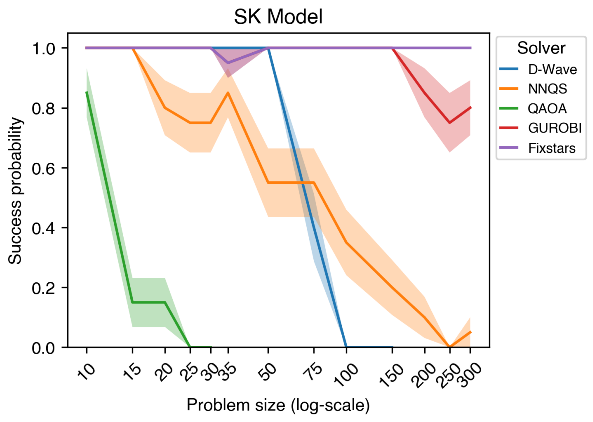

(b) Success probability

Figure 5.5: Performance of different solvers for SK model by problem size

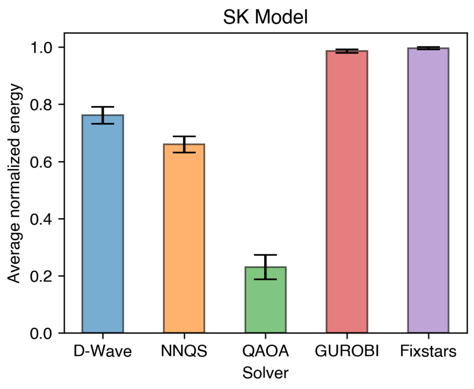

(a) Normalized energy

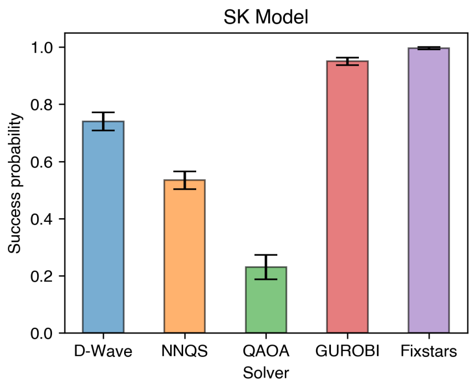

(b) Success probability

Figure 5.6: Average performance of different solvers for SK model

The D-Wave solver performs well up to $n = 50$ with a success probability of 1. For larger problem sizes, the performance of the D-Wave solver drops off sharply. The NNQS solver performs well up to $n = 15$, with the success probability gradually decreasing with increasing problem size. The QAOA solver performs poorly for all problem sizes, possibly as the SK model presents a more difficult optimisation problem. Between the classical solvers, the Fixstars QUBO solver performs better than the GUROBI optimiser except for $n = 35$. However, this is likely due to variance in the randomly generated dataset. Both classical solvers generally outperform the quantum-inspired solvers.

Overall, the D-Wave annealer has the highest average normalised energy and success probability among the three quantum-inspired solvers. The NNQS is slightly worse in both metrics, while the QAOA solver performs poorly for both metrics. Both classical solvers outperform the quantum-inspired solvers.

5.3 Time-Constrained Solver Comparison

We also measured the average runtime for each solver by problem type and size shown in Figure 5.7. Runtimes split by problem type can be found in Appendix D

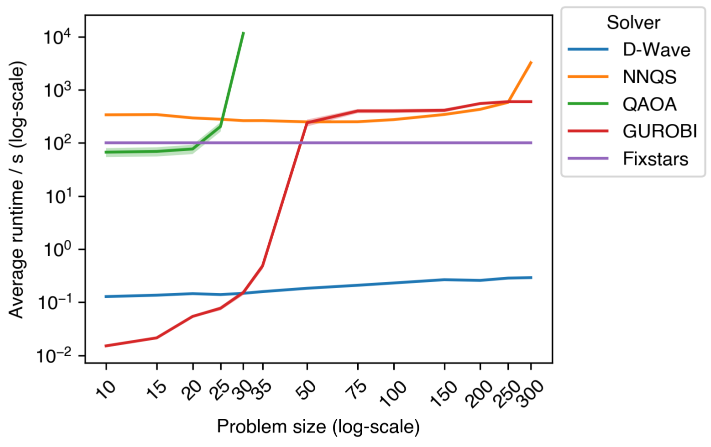

Figure 5.7: Average runtime taken by different solvers for QUBO problems by size. Both problem size and average runtime are plotted in log scale.

The runtime of the D-Wave solver increases approximately linearly from 0.128s for

$n = 10$ to 0.184s for $n = 50$ and 0.292s for $n = 300$. The runtime of the NNQS solver remains from 250s to 350s for n between 10 and 200 but increases sharply for $n \geq 250$, which could be due to memory issues with the GPU or a longer sampling time. The QAOA solver's runtime remains stable from $n = 10$ to $n = 20$ at around 38s. However, it increases rapidly to 6847s at $n = 30$ due to the need for many more iterations for the parameters to converge and greater computational resources for the simulation.

The GUROBI optimiser was set with a maximum time limit of 600s but could finish solving before the time limit for most problems with $n \leq 35$. The Fixstars solver was configured with a time limit of 100s, the maximum possible duration, with each solve utilising the entire time limit.

Since the D-Wave solver seems to be the most promising quantum-inspired solver, we conducted an additional experiment where the runtimes were matched. Using the average runtime of the D-Wave solver, we measured the performance of the D-Wave solver against the GUROBI and Fixstars solvers to see if the D-Wave solver could outperform the classical solvers when limited to the same runtime. The classical solvers were run with a runtime limit equal to the average runtime by the D-Wave solver for problems of equivalent type and size shown in Table 5.1.

n	10	15	20	25	30	35	50	75	100	150	200	250	300
NAE3SAT	0.133	0.135	0.141	0.149	0.138	0.156	0.173	0.184	0.201	0.243	0.259	0.286	0.292
Max-cut	0.127	0.136	0.1560	0.130	0.155	0.160	0.183	0.223	0.247	0.278	-	-	-
SK model	0.125	0.137	0.140	0.140	0.150	0.161	0.195	0.221	0.245	0.278	-	-	-

Table 5.1: Average runtime (seconds) of the D-Wave solver by problem type and size. Dashes indicate that the D-Wave solver could not embed problems of that size.

The average performance is shown in Figure 5.8. For each problem type, the performance of the GUROBI solver drops before the D-Wave solver, and there are problem types and sizes where the D-Wave solver outperforms the GUROBI solver. The D-Wave solver outperforms the GUROBI solver for the NAE3SAT problems with $n = 50, 75$, max-cut problems with $n = 30, 35$, and the SK model with $n = 20, 35$. However, when the problem sizes increase even further, the D-Wave solver underperforms the classical solvers, possibly due to the increased noise of the quantum annealer. The Fixstars solver remains the best-performing solver across all problem types for almost all sizes, even when the runtime is matched with the D-Wave solver. The results show that the D-Wave solver can outperform the GUROBI solver for specific problem sizes when the runtime is matched, a new result that has not been shown in the literature.

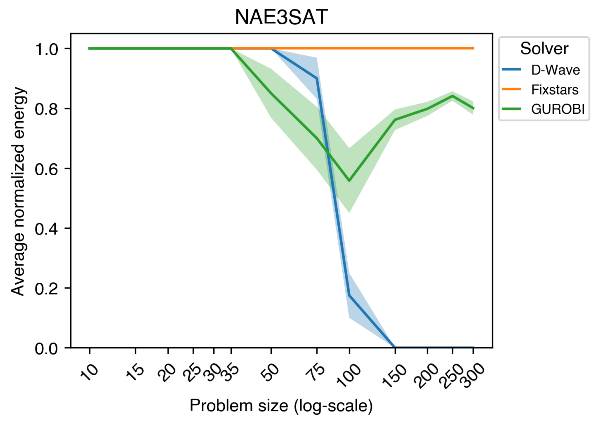

(a) NAE3SAT

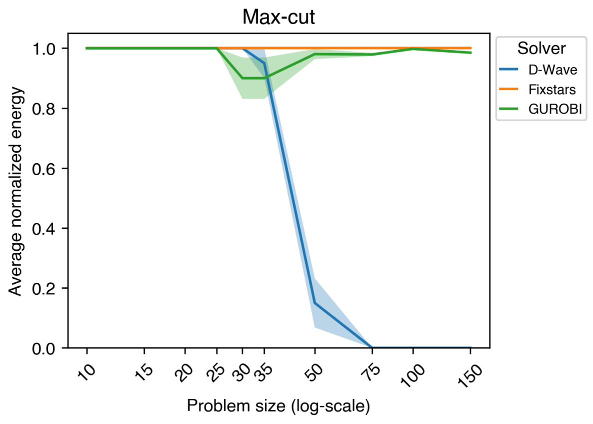

(b) Max-cut

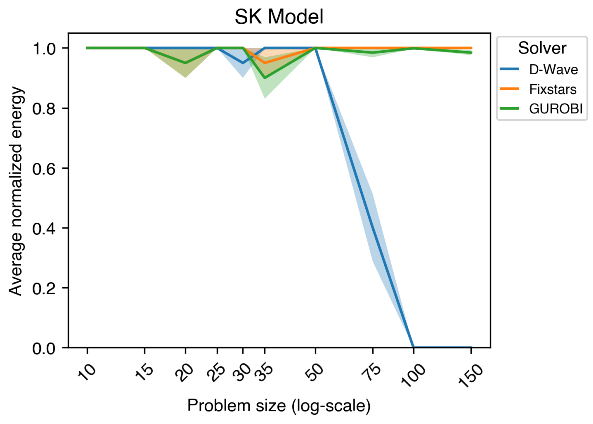

(c) SK model

Figure 5.8: Average normalised energy of D-Wave solver against the GUROBI and Fixstars solvers by problem type and size

5.4 Additional Solver Information

Additional D-Wave and QAOA solver information was recorded during the benchmarking experiments. This information helps quantify the difficulty of a QUBO problem for a particular solver and could be used to classify different types of QUBO problems.

5.4.1 D-Wave

For the D-Wave solver, we recorded the average number of embedded qubits shown in Table 5.2, generated during the minor embedding phase when a single qubit is split into a chain. The number of embedded qubits increases at different rates for different problem types and could be a metric for the difficulty of the annealing problem. The number of embedded qubits also limits the problems the D-Wave solver can handle since the QPU only has $\sim$ 5000 qubits.

n	10	15	20	25	30	35	50	75	100	150	200	250	300
NAE3SAT	15.15	27.90	42.20	58.85	80.90	102.25	184.05	379.65	622.15	1381.00	2322.65	3756.20	4493.60
Max-cut	12.70	25.95	45.45	69.90	102.60	142.50	304.05	706.05	1290.00	3087.95	-	-	-
SK model	17.05	35.80	54.50	87.65	121.15	169.80	331.60	739.45	1338.65	2995.25	-	-	-

Table 5.2: Average number of embedded qubits for the D-wave solver by problem type and size

5.4.2 QAOA

For the QAOA solver, we recorded the number of quantum gates and the circuit depth, shown in Table 5.3 and Table 5.4, respectively, which can help quantify the complexity of the quantum circuit used and the requirements needed for a quantum computer to run the QAOA solver.

n	10	15	20	25	30
NAE3SAT	77.75	127.80	181.50	235.20	292.30
Max-cut	75.00	131.00	200.00	281.00	375.00
SK model	95.00	180.00	290.00	425.00	585.00

Table 5.3: Average number of quantum gates in the quantum circuit used by the QAOA solver by problem type and size

n	10	15	20	25	30
NAE3SAT	18.65	25.30	30.70	35.15	40.00
Max-cut	19.00	28.05	36.50	45.60	55.05
SK model	22.00	32.00	42.00	52.00	62.00

Table 5.4: Average depth of the quantum circuit used by the QAOA solver by problem type and size

5.5 Conclusion

Table 5.5 and Table 5.6 show the average normalised energy and success probability for different solvers for each dataset and also the average value across all datasets. Among the three quantum-inspired solvers, the NNQS solver has the highest normalised energy for the NAE3SAT and max-cut dataset, while the D-Wave solver has the highest normalised energy for the SK model performance. The NNQS solver also has the highest normalised energy when averaged across the three datasets.

The QAOA solver has the highest success probability for the NAE3SAT dataset, however, it can only handle problems with up to 30 variables. The D-Wave solver has the highest success probability for the max-cut and SK model datasets while doing better than the NNQS solver for the NAE3SAT dataset. When averaged across the three datasets, the D-Wave solver has the highest success probability.

The NNQS solver tends to do better in normalised energy since it minimises the energy expectation value and consistently finds low-energy solutions. Conversely, the D-Wave solver is better at finding the best solution. The two solvers have different strengths and may be suited for different optimisation tasks.

Across all datasets and metrics, the Fixstars solver has the best performance, consistently returning the best solutions for almost all problem types and sizes. The GUROBI solver also does well, except for large problems ($n \geq 250$). When the runtimes are matched, the D-Wave solver can outperform the GUROBI solver for specific problem sizes but still underperforms the Fixstars solver.

	D-Wave	NNQS	QAOA	GUROBI	Fixstars
NAE3SAT	0.617	**0.755**	0.640	0.983	1.00
Max-cut	0.610	**0.753**	0.190	0.991	1.00
SK model	**0.761**	0.664	0.230	0.990	1.00
Average	0.663	**0.724**	0.353	0.988	1.00

Table 5.5: Average normalised energy for different solvers

	D-Wave	NNQS	QAOA	GUROBI	Fixstars
NAE3SAT	0.615	0.538	**0.640**	0.858	1.00
Max-cut	**0.610**	0.585	0.190	0.931	1.00
SK model	**0.740**	0.538	0.230	0.954	1.00
Average	**0.655**	0.554	0.353	0.914	1.00

Table 5.6: Success probability for different solvers

Chapter 6

NNQS exploration

This chapter explores the performance of different architectures and training schedules that can be used to train the NNQS solver. All experiments in this section were run on a subset of the entire dataset with problem sizes of $10, 25, 50, 75, 200, 250$ and 10 problems for each problem type and size.

6.1 Architectures and Training Schedules

We will utilise the Restricted Boltzmann Machine (RBM) and the Multilayer Perceptron (MLP) as the architecture for NNQS. For a given input problem with n variables, the RBM model will have n visible nodes and $5n$ hidden nodes, while the MLP will have n input nodes, 1 hidden layer of size $5n$ and 1 positive real output node. The RBM uses the sigmoid function, while the MLP uses the ReLU activation function and a sigmoid function as the output function. We use Gibbs sampling for the RBM and Metropolis sampling for the MLP which are detailed in section 2.4.

We will also compare three training schedules for the NNQS solver—progressive, direct, and continuous. The progressive training algorithm follows Algorithm 2 and has been utilised in previous experiments. In progressive training, the normalised anneal fraction

s is incremented by 0.1, and the NNQS is trained until convergence each time. In direct training, described in Algorithm 3, s is held constant at 1 for all epochs. In continuous training, described in Algorithm 4, s is gradually increased every iteration and the NNQS is not trained to convergence. All schedules use at most 1000 iterations.

Algorithm 2 NNQS Progressive Schedule

```
for $s \in [0.1, 1.0]$ step 0.1 do
    Set $H(s) \leftarrow A(s)\hat{H}_0 + B(s)\hat{H}_c$;
    Train NNQS on $H(s)$ until convergence or until epoch limit of 100 is reached;
```

Algorithm 3 NNQS Direct Schedule

```
Set $H \leftarrow B(1)\hat{H}_c$;
Train NNQS on $H$ until convergence or until epoch limit of 1000 is reached;
```

Algorithm 4 NNQS Continuous Schedule

```
for $s \in [0.001, 1.0]$ step 0.001 do
    Set $H(s) \leftarrow A(s)\hat{H}_0 + B(s)\hat{H}_c$;
    Train NNQS on $H(s)$ for 1 epoch;
```

Direct training is a baseline for training a neural network with the cost function as the problem Hamiltonian for the entire training period. Progressive training most closely resembles the quantum annealing process, where the system is kept at the ground state by training until convergence after each increment of s. Continuous training slowly increments s but does not train until convergence.

6.2 Results and Discussion

We present the performance metrics for each dataset, accompanied by error bars representing the unbiased standard error of the mean. Graphs with problem sizes on the x-axis are plotted with a log scale. The performance by dataset and problem size is shown in Appendix C.

6.2.1 NAE3SAT

For the NAE3SAT dataset, the continuous training scheme with the RBM performs the best in average performance and success probability when averaged across all problem sizes, shown in Figure 6.1. The RBM, with progressive training, and the MLP, with continuous training, also perform well.

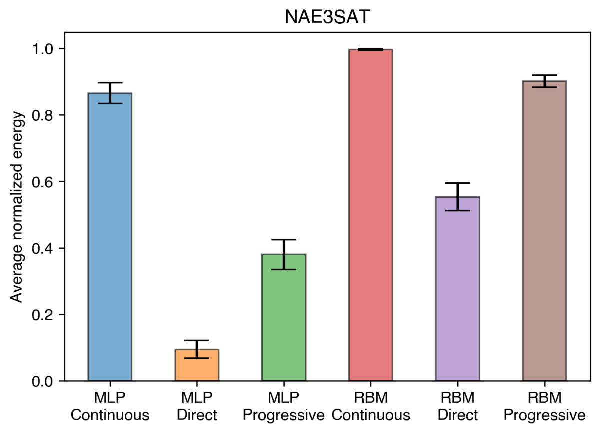

(a) Normalized energy

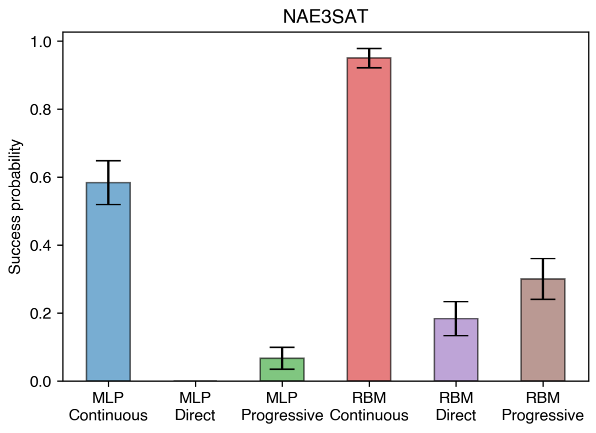

(b) Success probability

Figure 6.1: Average performance of different NNQS types for NAE3SAT

6.2.2 Max-cut

For the maxcut dataset, the continuous training algorithm with the RBM again performs the best in average performance and success probability when averaged across all sizes, shown in Figure 6.2. The RBM, with progressive training, and the MLP, with continuous training, also perform well. However, the performance gap between the top three solvers is relatively small, implying that the max-cut problem is easier than the NAE3SAT problem.

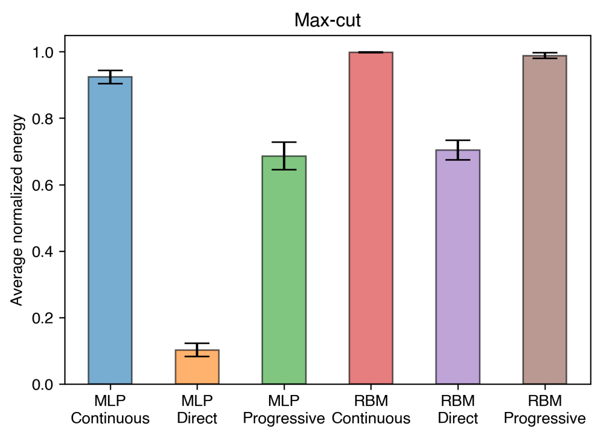

(a) Normalized energy

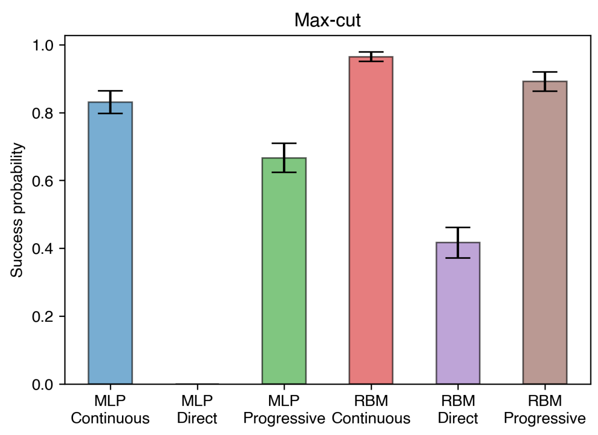

(b) Success probability

Figure 6.2: Average performance of different NNQS types for max-cut

6.2.3 SK model

For the SK model dataset, the continuous training algorithm with the RBM again performs the best in average performance and success probability when averaged across all sizes, shown in Figure 6.3. The RBM, with progressive training also perform well in both metrics.

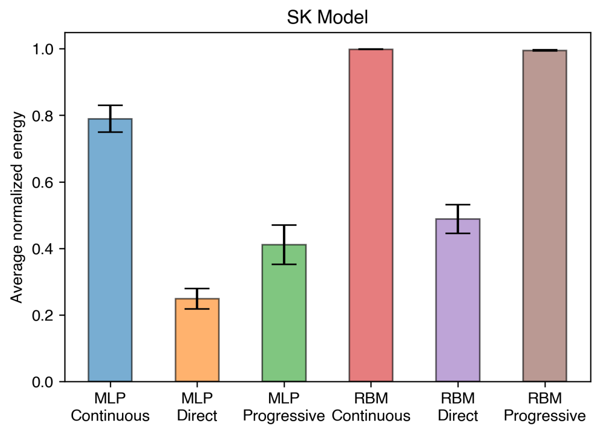

(a) Normalized energy

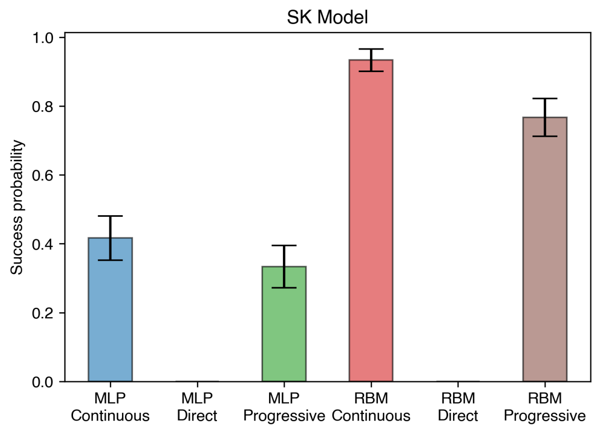

(b) Success probability

Figure 6.3: Average performance of different NNQS types for SK model

6.3 Conclusion

Table 6.1 and Table 6.2 summarises the average normalised energy and success probability for different types of NNQS for each dataset and also the average across all datasets.

Comparing the two architectures, RBM performs better than MLP in average normalised energy and success probability for all datasets and training schemes. In terms of training schemes, direct training performs the worst among the three, and continuous training performs slightly better than progressive training. Using the RBM with a continuous training scheme gives the highest normalised energy and success probability across all datasets.

The RBM likely performs better as it uses Gibbs sampling, which helps the neural network approximate the wave function more closely. The Gibbs sampling method also allows for multiple-bit flips in each iteration and is thus able to explore a larger state space.

Even though progressive training more closely mimics the quantum annealing process in D-wave solvers, the sudden change of Hamiltonian may have led to large gradient terms that may have made it more difficult for the network to converge, leading to poorer training. Continuous training gradually changes the Hamiltonian, which limits the gradient magnitudes and may result in better training. Direct training is expected to perform poorly as it tends to get stuck in local minima.

	MLP			RBM		
	Continuous	Direct	Progressive	Continuous	Direct	Progressive
NAE3SAT	0.866	0.118	0.352	**0.997**	0.511	0.910
Max-cut	0.924	0.102	0.686	**0.998**	0.704	0.988
SK model	0.790	0.248	0.411	**0.999**	0.488	0.995
Average	0.860	0.156	0.483	**0.998**	0.568	0.965

Table 6.1: Average normalised energy for different NNQS types

	MLP			RBM		
	Continuous	Direct	Progressive	Continuous	Direct	Progressive
NAE3SAT	0.583	0.029	0.062	**0.950**	0.167	0.364
Max-cut	0.831	0.000	0.667	**0.965**	0.417	0.892
SK model	0.417	0.000	0.333	**0.933**	0.000	0.767
Average	0.610	0.010	0.354	**0.949**	0.194	0.674

Table 6.2: Success probability for different NNQS types

Chapter 7

Conclusion

This chapter summarises our study's contributions and limitations. It also makes recommendations for further work that future projects could investigate.

7.1 Contributions

In this study, we have benchmarked 5 QUBO solvers:

1. D-Wave Quantum Annealer
2. Neural Network Quantum States (NNQS)
3. Quantum Approximate Optimization Algorithm (QAOA)
4. GUROBI Optimizer
5. Fixstars Amplify QUBO Solver

We used three types of QUBO problems: not-all-equal 3-satisfiability (NAE3SAT), max-cut, and Sherrington-Kirkpatrick model (SK model) problems as datasets to evaluate the solvers' performance.

Our results show that the D-Wave and NNQS solvers perform the best among the quantum-inspired solvers. The NNQS solver is generally better than the D-Wave solver except for the SK model dataset. The QAOA solver achieves generally poor performance across datasets and is not comparable due to the limitations on problem size. All three quantum-inspired solvers underperform the two classical solvers, with the simulated-annealing-based Fixstars solver achieving the best performance for all datasets.

When the runtimes of the D-Wave, GUROBI, and Fixstars solvers were matched, the D-Wave solver could outperform the GUROBI solver for specific ranges of problem sizes. This inspires further development of quantum annealers that can handle larger problems with dense connectivity.

We also investigated the NNQS solver with different architectures and training algorithms. The Restricted Boltzmann Machine (RBM) and the Multilayer Perceptron (MLP) were used as the underlying neural networks along with three different training algorithms—progressive, direct, and continuous. We found that the RBM with a continuous training scheme performs best across all datasets.

7.2 Limitations and Future Work

The primary constraint of our study came from the limitations of the QAOA solver, which was intended to be run on a gate-based quantum computer. Due to restricted availability, we could only use a simulator capable of handling only up to 30 variables. However, as the QAOA simulator does not model quantum noise and the results from the QAOA solver for small problems are not promising, QAOA on an actual quantum device would likely perform even worse for larger problems and is thus not too interesting to benchmark in the current NISQ era. Another limitation was that there were many parameters for each solver that we did not have the resources to optimise for, such as the annealing time for the D-Wave solver and various forms of the QAOA Ansatz. These might be more suitable for a future project that optimises one specific QUBO solver.

Future studies can explore more QUBO problem types and attempt to classify problems that are difficult for annealing-based solvers, such as quantum annealers and simulated annealers, but easier for other solvers like the QAOA solver. When gate-based quantum computers are readily available, the QAOA solver with larger p values ($p > 1$) could also be benchmarked, which has been shown to perform better but requires more computational resources.

For further work with NNQS, future studies could investigate if more modern machine learning models, such as Graph Neural Networks or Attention-based Neural Networks, can be used as the underlying architecture for NNQS and whether they provide better performance.

Future studies could also investigate whether NNQS closely approximates the wave function of a D-Wave solver in the quantum annealing process. A quench of the D-Wave annealing process can help take a snapshot of the intermediate state, which can be compared to the intermediate sampling results from the NNQS solver. Extra information is included in Appendix E.

References

Achlioptas, D., Chtcherba, A., Istrate, G., & Moore, C. (2001). The phase transition in 1-in-k sat and nae 3-sat. *Proceedings of the Annual ACM-SIAM Symposium on Discrete Algorithms*, , 05, 2001.

Alidaee, B. (2009). Minimizing absolute and squared deviation of completion times from due dates. *Production and Operations Management*, *3*, 01, 2009, 133 – 147.

Alidaee, B., Glover, F., Kochenberger, G., & Rego, C. (2005). A new modeling and solution approach for the number partitioning problem. *JAMDS*, *9*, 01, 2005, 113–121.

Barahona, F. (1982). On the computational complexity of ising spin glass models. *Journal of Physics A: Mathematical and General*, *15*(10)1982, 3241.

Baxter, R. J. (2016). *Exactly solved models in statistical mechanics.* Elsevier.

Blekos, K., Brand, D., Ceschini, A., Chou, C.-H., Li, R.-H., Pandya, K., & Summer, A. (2024). A review on quantum approximate optimization algorithm and its variants. *Physics Reports*, *1068*2024, 1–66.

Born, M., & Fock, V. (1928). Beweis des adiabatensatzes. *Zeitschrift für Physik A Hadrons and Nuclei*, *51*, 03, 1928, 165–180.

Carleo, G., & Troyer, M. (2017). Solving the quantum many-body problem with artificial neural networks. *Science*, *355*, 02, 2017, 602.

Cipra, B. A. (1987). An introduction to the ising model. *The American Mathematical Monthly*, *94*(10)1987, 937–959.

D. J. Thouless, P. W. A., & Palmer, R. G. (1977). Solution of 'solvable model of a spin glass'. *The Philosophical Magazine: A Journal of Theoretical Experimental and Applied Physics*, *35*(3)1977, 593–601.

D-Wave Systems (2024a). Annealing implementation and controls. `https://docs.dwavesys.com/docs/latest/c_qpu_annealing.html`. Accessed: 2024-01-04.

D-Wave Systems (2024b). Minor-embedding. `https://docs.ocean.dwavesys.com/en/stable/concepts/embedding.html`. Accessed: 2024-01-04.

D-Wave Systems (2024c). Qpu-specific characteristics. `https://docs.dwavesys.com/docs/latest/doc_physical_properties.html`. Accessed: 2024-01-04.

D-Wave Systems (2024d). Solver docs. `https://docs.ocean.dwavesys.com/en/stable/docs_dimod/reference/generated/dimod.generators.random_nae3sat.html`. Accessed: 2024-01-04.

Denchev, V. S., Boixo, S., Isakov, S. V., Ding, N., Babbush, R., Smelyanskiy, V., Martinis, J., & Neven, H. (2016). What is the computational value of finite-range tunneling? *Physical Review X*, *6*(3)2016, 031015.

Dunning, I., Gupta, S., & Silberholz, J. (2018). What works best when? a systematic evaluation of heuristics for max-cut and qubo. *INFORMS Journal on Computing*, *30*, 08, 2018, 608–624.

Farhi, E., Goldstone, J., & Gutmann, S. (2014). A quantum approximate optimization algorithm.

Farhi, E., Goldstone, J., Gutmann, S., Lapan, J., Lundgren, A., & Preda, D. (2001). A quantum adiabatic evolution algorithm applied to random instances of an np-complete problem. *Science*, *292*(5516)2001, 472–475.

Geman, S., & Geman, D. (1984). Stochastic relaxation, gibbs distributions, and the bayesian restoration of images. *IEEE Transactions on pattern analysis and machine intelligence*, *6*1984, 721–741.

Glover, F., Kochenberger, G., Hennig, R., & Du, Y. (2022). Quantum bridge analytics i: a tutorial on formulating and using qubo models. *Annals of Operations Research*, *314*, 07, 2022.

Gomes, J., McKiernan, K. A., Eastman, P., & Pande, V. S. (2019). Classical quantum optimization with neural network quantum states. *arXiv preprint arXiv:1910.10675*, 2019.

Griffiths, D. J., & Schroeter, D. F. (2018). *Introduction to quantum mechanics.* Cambridge University Press, 3 edition.

Gurobi Optimization, LLC (2023). Gurobi Optimizer Reference Manual.

Harris, R., Sato, Y., Berkley, A., Reis, M., Altomare, F., Amin, M., Boothby, K., Bunyk, P., Deng, C., Enderud, C., Huang, S., Hoskinson, E., Johnson, M., Ladizinsky, E., Ladizinsky, N., Lanting, T., Li, R., Medina, T., Molavi, R., & Yao, J. (2018). Phase transitions in a programmable quantum spin glass simulator. *Science (New York, N.Y.)*, *361*, 07, 2018, 162–165.

Hastings, W. K. (1970). Monte carlo sampling methods using markov chains and their applications. *Biometrika*, *57*(1)1970, 97–109.

Horn, R. A., & Johnson, C. R. (1990). *Matrix analysis.* Cambridge University Press.

Huang, T., Xu, J., Luo, T., Gu, X., Goh, R., & Wong, W. (2023). Benchmarking quantum(-inspired) annealing hardware on practical use cases. *IEEE Transactions on Computers*, *72*(06), 06, 2023, 1692–1705.

IBM (2024). Transpiler. `https://docs.quantum.ibm.com/api/qiskit/transpiler`. Accessed: 2024-01-04.

Ising, E. (1925). Beitrag zur theorie des ferromagnetismus. *Zeitschrift für Physik*, *31*(1)1925, 253–258.

Kadowaki, T., & Nishimori, H. (1998). Quantum annealing in the transverse ising model. *Physical Review E*, *58*(5)1998, 5355.

Khandoker, S. A., Abedin, J. M., & Hibat-Allah, M. (2023). Supplementing recurrent neural networks with annealing to solve combinatorial optimization problems. *Machine Learning: Science and Technology*, *4*(1)2023, 015026.

Kirkpatrick, S., Gelatt, C. D., & Vecchi, M. P. (1983). Optimization by simulated annealing. *Science*, *220*(4598)1983, 671–680.

Kochenberger, G., Hao, J.-K., Glover, F., Lewis, M., Lu, Z., Wang, H., & Wang, Y. (2014). The unconstrained binary quadratic programming problem: A survey. *Journal of Combinatorial Optimization*, *28*, 07, 2014.

Kochenberger, G., Hao, J.-K., Lu, Z., Wang, H., & Glover, F. (2013). Solving large scale max cut problems via tabu search. *Journal of Heuristics*, *19*, 08, 2013.

Kolmogorov, A. N. (1957). On the representation of continuous functions of many variables by superposition of continuous functions of one variable and addition. *Doklady Akademii Nauk*, Vol. 114 (pp. 953–956), Russian Academy of Sciences, 1957.

Kramers, H. A., & Wannier, G. H. (1941). Statistics of the two-dimensional ferromagnet. part i. *Phys. Rev.*, *60*, 08, 1941, 252–262.

Kurowski, K., Pecyna, T., Slysz, M., Rozycki, R., Waligora, G., & Weglarz, J. (2023). Application of quantum approximate optimization algorithm to job shop scheduling problem. *European Journal of Operational Research*, *310*, 03, 2023.

Lanczos, C. (1950). An iteration method for the solution of the eigenvalue problem of linear differential and integral operators. *J. Res. Natl. Bur. Stand. B*, *45*1950, 255–282.

Lang, J., Zielinski, S., & Feld, S. (2022). Strategic portfolio optimization using simulated, digital, and quantum annealing. *Applied Sciences*, *12*(23)2022.

Lehoucq, R., Sorensen, D., & Yang, C. (1998). *Arpack users' guide: Solution of large-scale eigenvalue problems with implicitly restarted arnoldi methods.* Software, Environments, and Tools. Society for Industrial and Applied Mathematics.

Lucas, A. (2014). Ising formulations of many np problems. *Frontiers in Physics*, *2*, 02, 2014, 5.

Lykov, D., Wurtz, J., Poole, C., Saffman, M., Noel, T., & Alexeev, Y. (2023). Sampling frequency thresholds for the quantum advantage of the quantum approximate optimization algorithm. *npj Quantum Information*, *9*(1)2023, 73.

McGeoch, C., & Farré, P. (2021). *The advantage system: Performance update* (Technical report). D-Wave Systems.

Onsager, L. (1944). Crystal statistics. i. a two-dimensional model with an order-disorder transition. *Phys. Rev.*, *65*, 02, 1944, 117–149.

Otaki, K., Okada, A., & Yoshida, H. (2023). Experimental study on the information disclosure problem: Branch-and-bound and qubo solver. *Frontiers in Applied Mathematics and Statistics*, *9*, 03, 2023.

Pelofske, E., Bärtschi, A., & Eidenbenz, S. (2023). Quantum annealing vs. qaoa: 127 qubit higher-order ising problems on nisq computers. In A. Bhatele, J. Hammond, M. Baboulin, & C. Kruse (Eds.), *High Performance Computing* (pp. 240–258), 2023: Springer Nature Switzerland.

Punnen, A. P. (2022). *The quadratic unconstrained binary optimization problem.* Springer International Publishing.

Qiskit contributors (2023). Qiskit: An open-source framework for quantum computing.

Quintero, R., & Zuluaga, L. (2022). Qubo formulations of combinatorial optimization problems for quantum computing devices.

Rieffel, E., Venturelli, D., O'Gorman, B., do, M., Prystay, E., & Smelyanskiy, V. (2014). A case study in programming a quantum annealer for hard operational planning problems. *Quantum Information Processing*, *14*, 07, 2014.

Rosenberg, G., Haghnegahdar, P., Goddard, P., Carr, P., Wu, J., & Lopez de Prado, M. (2016). Solving the optimal trading trajectory problem using a quantum annealer. *IEEE Journal of Selected Topics in Signal Processing*, *10*, 09, 2016, 1–1.

Tavares, G. (2008). *New algorithms for quadratic unconstrained binary optimization (qubo) with applications in engineering and social sciences.* PhD thesis, Rutgers University.

Tieleman, T. (2012). Lecture 6.5-rmsprop: Divide the gradient by a running average of its recent magnitude. `https://cir.nii.ac.jp/crid/1370017282431050757`.

Vert, D., Sirdey, R., & Louise, S. (2021). Benchmarking quantum annealing against "hard"instances of the bipartite matching problem. *SN Computer Science*, *2*(2), 02, 2021, 106.

Willsch, M., Willsch, D., Jin, F., De Raedt, H., & Michielsen, K. (2020). Benchmarking the quantum approximate optimization algorithm. *Quantum Information Processing*, *19*(7), 06, 2020, 197.

Yarkoni, S., Huck, A., Schuelldorf, H., Speitkamp, B., Tabrizi, M., Leib, M., Back, T., & Neukart, F. (2021). *Solving the shipment rerouting problem with quantum optimization techniques*, pp. 502–517. Springer, Cham.

Yarkoni, S., Raponi, E., Back, T., & Schmitt, S. (2022). Quantum annealing for industry applications: Introduction and review. *Reports on Progress in Physics*, *85*, 08, 2022.

Zen, R. A. M. (2021). *Transfer learning for neural-network quantum states.* PhD thesis, National University of Singapore. Available at `https://scholarbank.nus.edu.sg/handle/10635/224567`.

Zen, R. A. M., My, L., Tan, R., Hébert, F., Gattobigio, M., Miniatura, C., Poletti, D., & Bressan, S. (2020). Finding quantum critical points with neural-network quantum states. *European Conference on Artificial Intelligence*, 2020.

Zhou, L., Wang, S.-T., Choi, S., Pichler, H., & Lukin, M. D. (2020). Quantum approximate optimization algorithm: Performance, mechanism, and implementation on near-term devices. *Phys. Rev. X*, *10*, 06, 2020, 021067.

Appendix A

Reformulating the knapsack problem as a QUBO problem

This appendix explains an example of how a combinatorial optimisation problem with inequality constraints can be formalised as a QUBO problem. The knapsack problem is a classic combinatorial optimisation problem with a knapsack with integer weight limit $W > 0$ and n items, each with a weight $w_i > 0$ and profit $c_i > 0$. The problem seeks to find the optimal set of items to place in the knapsack to maximise total profit while not exceeding the weight limit. Formally, we have

$$\max \sum_{i=1}^{n} c_i x_i \tag{A.1}$$

$$\text{st.} \sum_{i=1}^{n} w_i x_i \leq W \tag{A.2}$$

$$x_i \in \{0, 1\}^n$$

The quantity A.1 refers to the total profit of the chosen items, and constraint A.2 keeps the total weight below the weight limit. To convert this optimisation problem into a QUBO problem, we can include the inequality constraint in our QUBO formulation by introducing slack variables, y_j's, which turn the inequality constraint into an equality constraint (Quintero & Zuluaga, 2022).

$$\max \sum_{i=1}^{n} c_i x_i \tag{A.3}$$

$$\text{st.} \sum_{i=1}^{n} w_i x_i = \sum_{j=1}^{W} j y_j \tag{A.4}$$

$$\sum_{j=1}^{W} y_j = 1 \tag{A.5}$$

$$x \in \{0,1\}^n, y \in \{0,1\}^W$$

The slack variables y_j track the total weight of the knapsack with $y_j = 1 \Leftrightarrow$ total weight is j. Constraint A.5 ensures that only one of y_j equals 1. With penalty parameters $C_1 > \sum_{i=1}^{n} c_i$ and $C_2 > \sum_{i=0}^{n} c_i$, we can formulate the following QUBO problem:

$$\max f(x,y) \coloneqq \sum_{i=1}^{n} c_i x_i - C_1 P_w^2 - C_2 P_n^2 \tag{A.6}$$

$$P_w \coloneqq \sum_{i=1}^{n} w_i x_i - \sum_{j=1}^{W} j y_j \tag{A.7}$$

$$P_n \coloneqq 1 - \sum_{j=1}^{W} y_j \tag{A.8}$$

$$x \in \{0,1\}^n, y \in \{0,1\}^W$$

Since the penalty parameters are larger than $\sum_{i=1}^{n} c_i$, the optimal solution to the QUBO problem must have $P_w = P_n = 0$. Hence, it ensures that exactly one of the $y_i = 1$ and the total weight is below the knapsack capacity. Since the optimal solution to the original knapsack must also have a total weight below the knapsack capacity, the value of x that solves the QUBO must also solve the original knapsack problem. We can also formulate this QUBO problem in terms of Q by following similar steps as subsection 2.1.1.

Appendix B

Curve fitting for NNQS

This section will describe how we obtained an analytical form of functions $A(s)$ and $B(s)$ as shown in Figure 4.2. The exact form is not provided in the D-wave documentation, but a set of 1000 discrete points is available from the documentation (D-Wave Systems, 2024c). A snapshot of the dataset is shown here:

s	$A(s)$ (GHz)	$B(s)$ (GHz)
0	0.000000	9.839417×10^{0}
0.001	0.001001	9.746483×10^{0}
0.002	0.002002	9.655434×10^{0}
...	...	...
0.998	0.997998	1.344913×10^{-9}
0.999	0.998999	1.293784×10^{-9}
1.000	1.000000	1.242656×10^{-9}

Table B.1: Discrete points of annealing functions $A(s)$ and $B(s)$

To obtain an analytical form, we utilised the curve fit function from the scipy library. First, we normalise by the maximum value in $B(s)$ as only the ratio of A and B is important. We fit an exponential decay form of $a_A \cdot e^{-b_A \cdot s} + c_A$ to $A(s)$ and a quadratic function $a_B \cdot s^2 + b_B \cdot s + c_B$ function to $B(s)$. The forms of the functions were chosen from the D-wave documentation (D-Wave Systems, 2024c). We obtain fitted constants of $a_A = 1.11, b_A = 7.06, c_A - 0.00569, a_B = 0.680, b_B = 0.288, c_B = 0.0305$. The fitted functions are shown in Figure B.1 along with the discrete values from the documentation and are found to be a good fit.

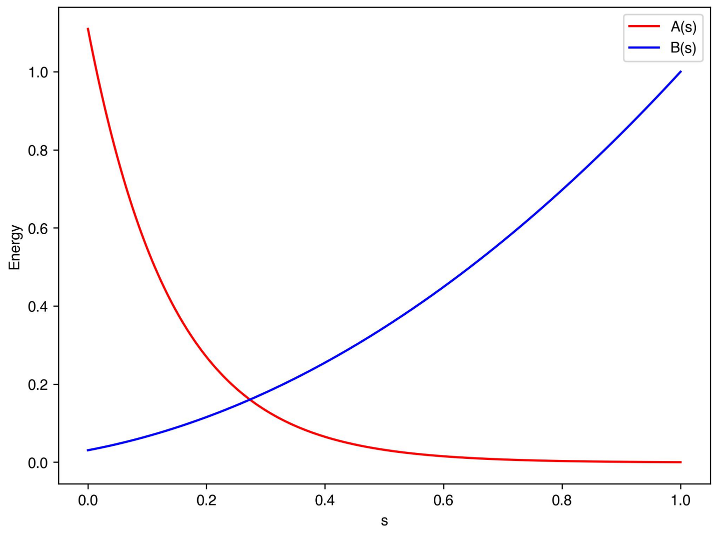

Figure B.1: Fitted $A(s)$ and $B(s)$ equations against the normalised annealing fraction s

Appendix C

NNQS exploration performance by sizes

C.1 NAE3SAT

Refer to Figure C.1.

C.2 Max-cut

Refer to Figure C.2.

C.3 SK model

Refer to Figure C.3.

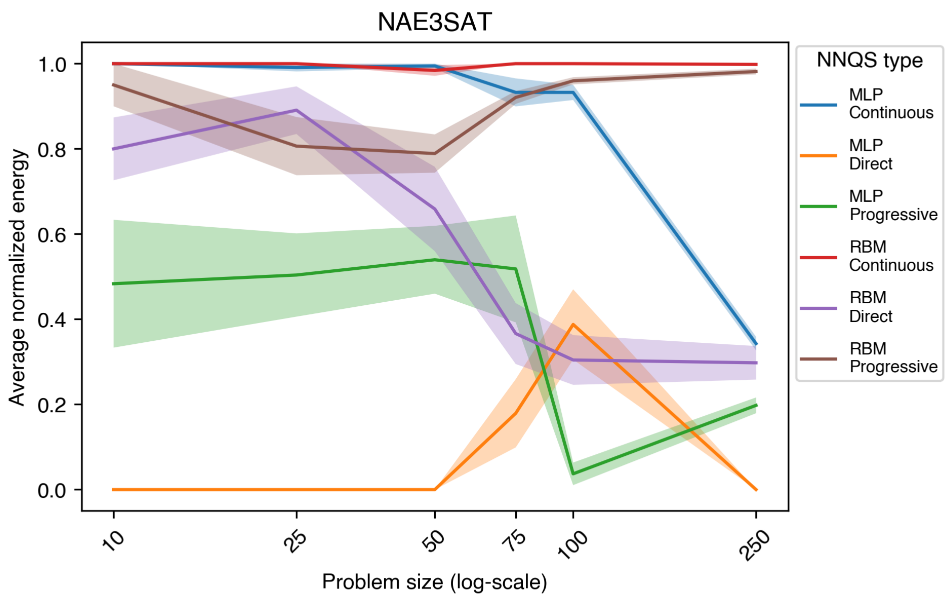

(a) Normalized energy

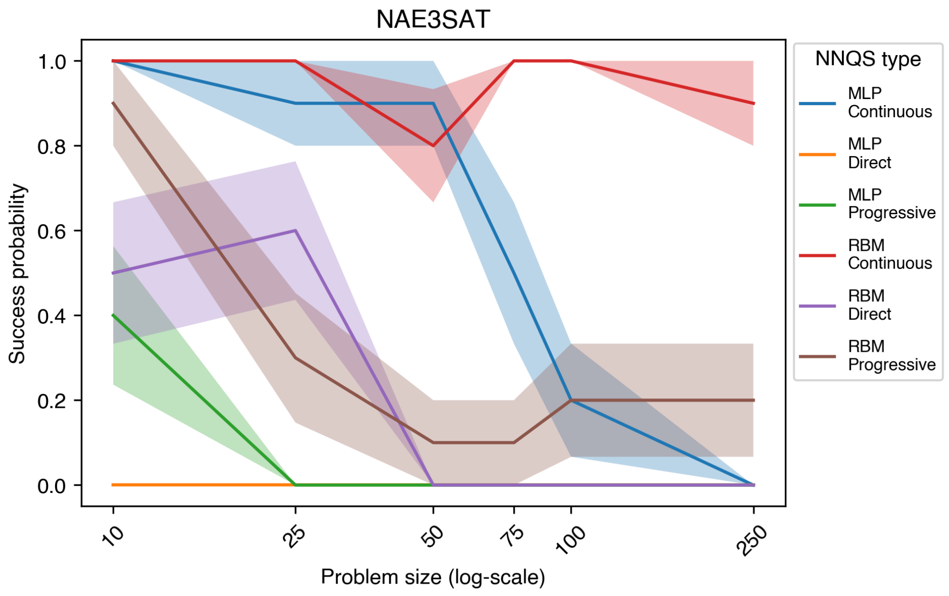

(b) Success probability

Figure C.1: Performance of different NNQS types for NAE3SAT by problem size

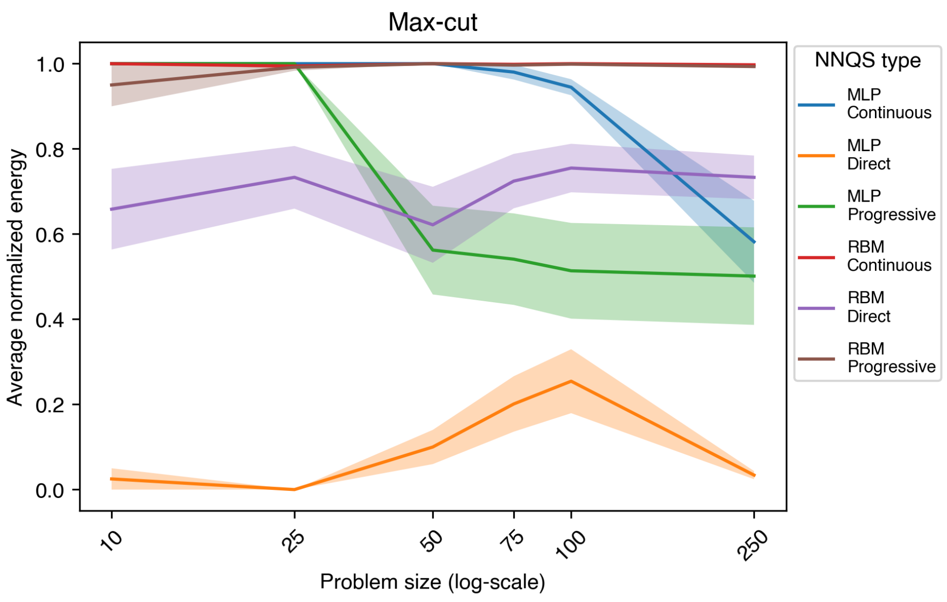

(a) Normalized energy

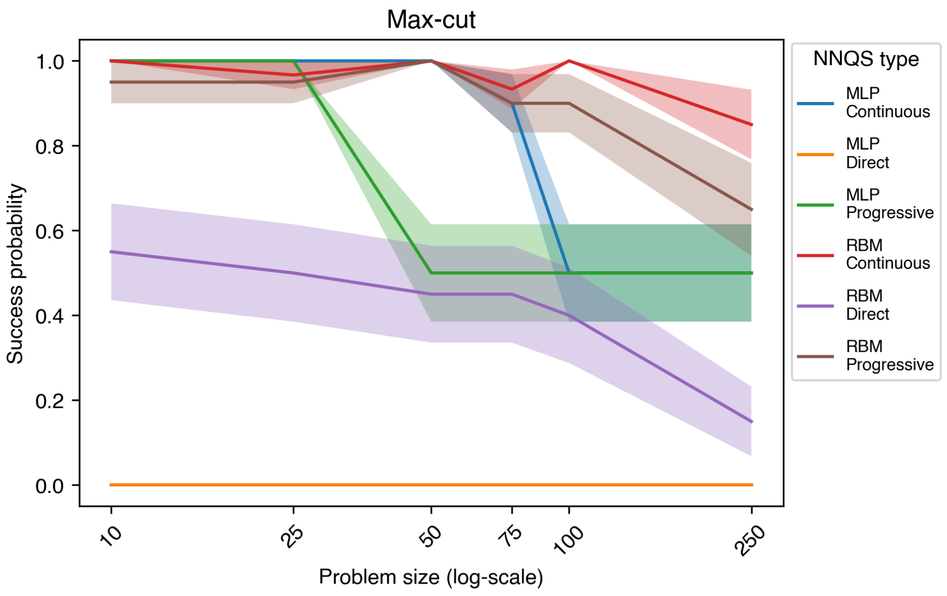

(b) Success probability

Figure C.2: Performance of different NNQS types for max-cut by problem size

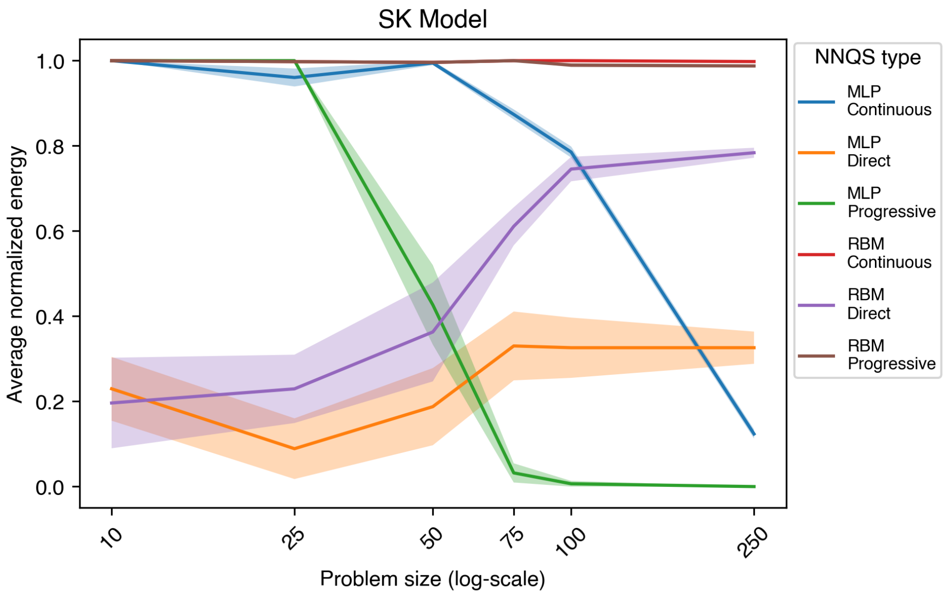

(a) Normalized energy

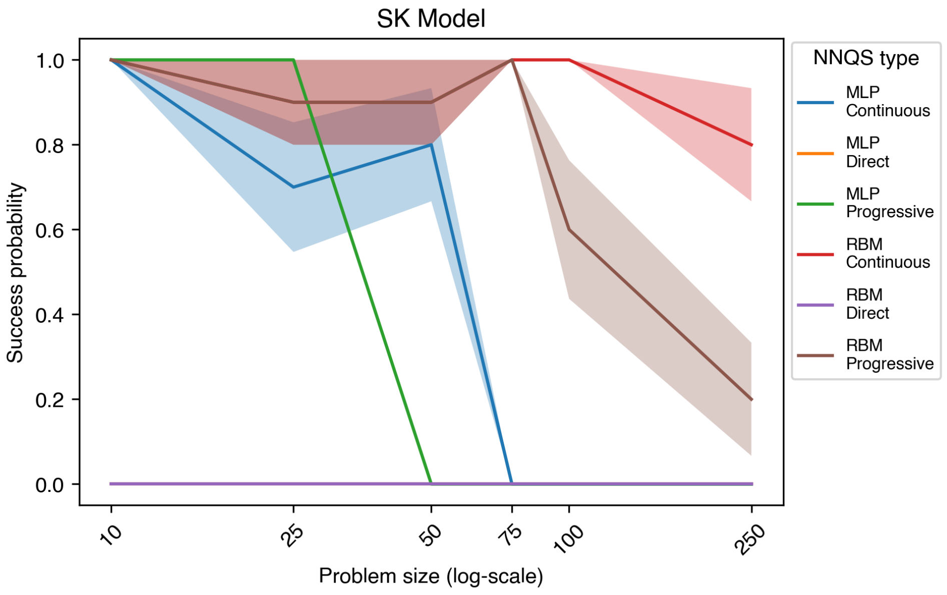

(b) Success probability

Figure C.3: Performance of different NNQS types for SK model by problem size

Appendix D

Average runtime of solvers by problem type and sizes

D.1 NAE3SAT

Figure D.1 shows the average runtime taken for NAE3SAT problems.

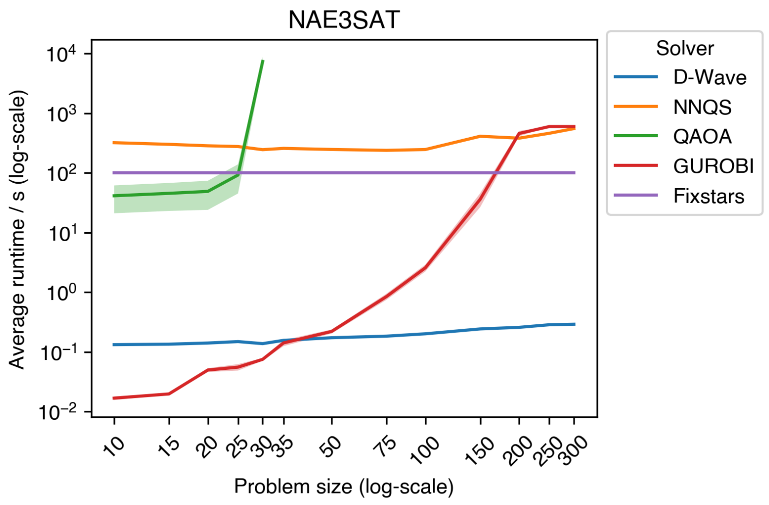

Figure D.1: Average runtime taken by different solvers for NAE3SAT by problem size

D.2 Max-cut

Figure D.2 shows the average runtime taken for max-cut problems.

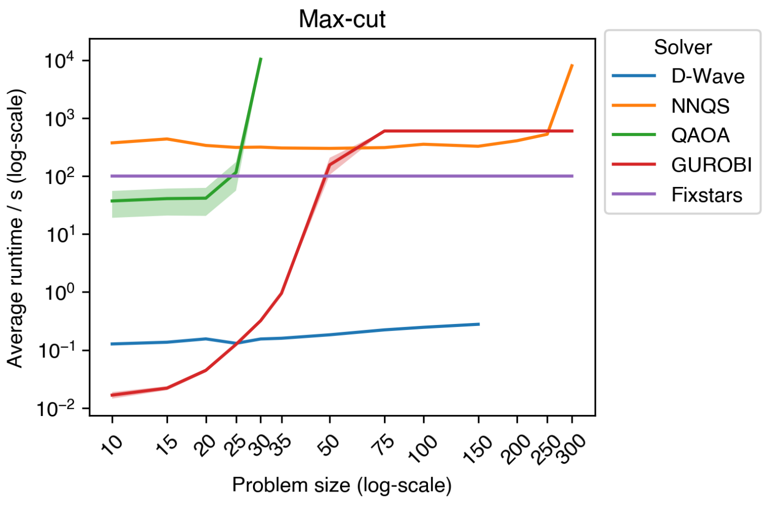

Figure D.2: Average runtime taken by different solvers for max-cut by problem size

D.3 SK model

Figure D.3 shows the average runtime taken for SK model problems.

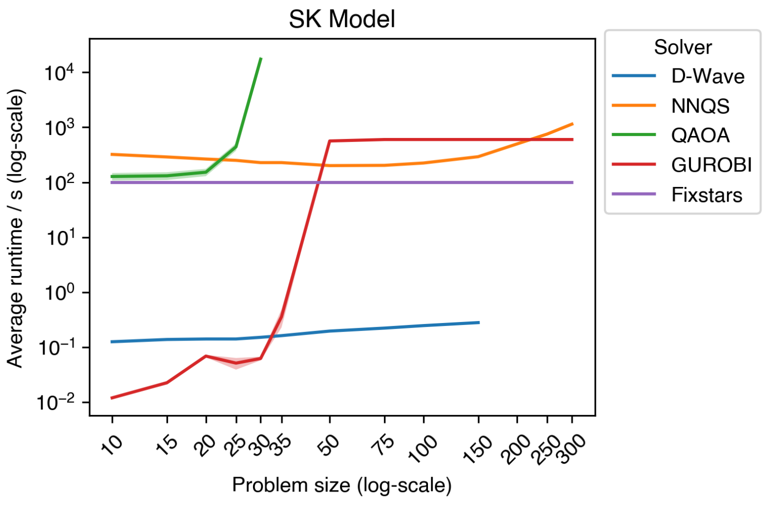

Figure D.3: Average runtime taken by different solvers for SK model by problem size

Appendix E

D-wave Quenching

A mid-anneal quench helps us identify the current state of the D-wave annealing by quickly increasing the value of s, the anneal fraction. By doing so, we change the system quickly compared to the system, which does not give the system enough time to evolve and freezes the current state. By measuring the distribution of states through repeated sampling, we can peek into the evolution of the wave function of the D-wave annealing setup and compare it to that of the NNQS.

We can quench the annealing process in a D-wave solver by specifying the anneal_schedule parameter by providing discrete points for (anneal fraction, time) (McGeoch & Farré, 2021). For example, a schedule that is $[(0.0, 0.0)(10.0, 0.5)(11.0, 1.0)]$, would mean a $10\mu s$ anneal until $s = 0.5$ then a $1\mu s$ quench until $s = 1$. For more information, refer to the D-wave documentation (D-Wave Systems, 2024a).